Cell Reports

Resource

Proteomics reveals distinct mechanisms regulating the release of cytokines and alarmins during pyroptosis

Graphical abstract

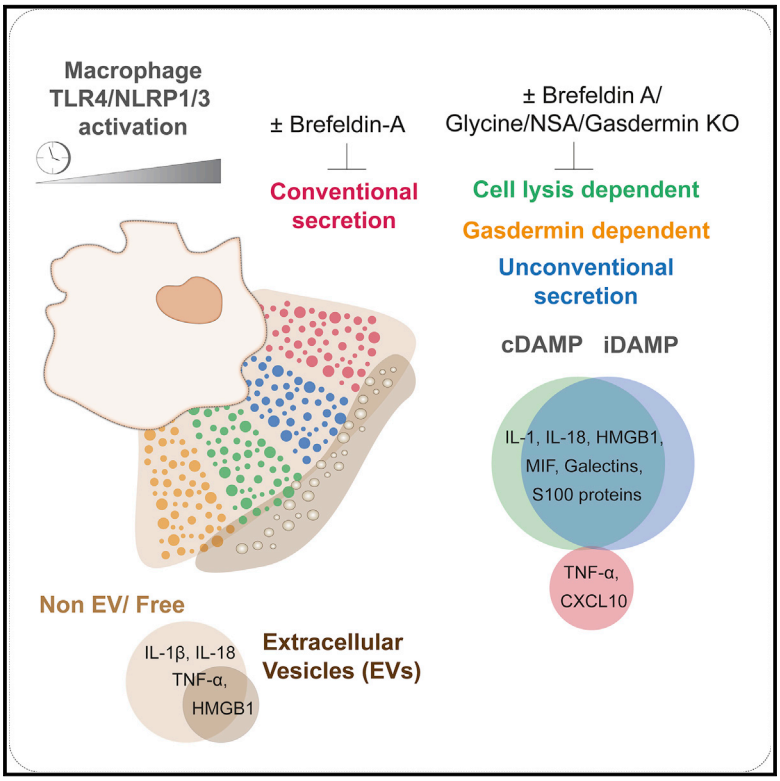

Authors

Kshiti Phulphagar, Lars I. Kühn, Stefan Ebner, Annika Frauenstein, Jonathan J. Swietlik, Jan Rieckmann, Felix Meissner

Correspondence

meissner@biochem.mpg.de

In brief

Using mass-spectrometry-based proteomics in combination with pharmacological and genetic perturbation, Phulphagar et al. dissect protein release during macrophage pyroptosis. The study defines proteins exiting cells through active secretion pathways, extracellular vesicles, organellar damage, and gasdermin pores and identifies the gasdermin-mediated release of multiple alarmins.

Highlights

- Mass spectrometry resource for inflammasome-activated protein release in macrophages
- Inhibition of inflammasome assembly and protein release by ER-Golgi disruption
- Dissection of protein release by gasdermin, organelle damage, and extracellular vesicles
- Identification of released constitutive and induced alarmins

Phulphagar et al., 2021, Cell Reports *34*, 108826
March 9, 2021
https://doi.org/10.1016/j.celrep.2021.108826

CellPress

Cell Reports

CellPress
OPEN ACCESS

Resource

Proteomics reveals distinct mechanisms regulating the release of cytokines and alarmins during pyroptosis

Kshiti Phulphagar,[1,2,3] Lars I. Kühn,[1,3] Stefan Ebner,[1] Annika Frauenstein,[1] Jonathan J. Swietlik,[1] Jan Rieckmann,[1] and Felix Meissner[1,2,4,*]

[1]Experimental Systems Immunology Laboratory, Max Planck Institute of Biochemistry, Martinsried, Germany
[2]Institute of Innate Immunity, Department of Systems Immunology and Proteomics, Medical Faculty, University of Bonn, Bonn, Germany
[3]These authors contributed equally
[4]Lead contact
*Correspondence: meissner@biochem.mpg.de
https://doi.org/10.1016/j.celrep.2021.108826

SUMMARY

A major pathway for proinflammatory protein release by macrophages is inflammasome-mediated pyroptotic cell death. As conventional secretion, unconventional secretion, and cell death are executed simultaneously, however, the cellular mechanisms regulating this complex paracrine program remain incompletely understood. Here, we devise a quantitative proteomics strategy to define the cellular exit route for each protein by pharmacological and genetic dissection of cellular checkpoints regulating protein release. We report the release of hundreds of proteins during pyroptosis, predominantly due to cell lysis. They comprise constitutively expressed and transcriptionally induced proteins derived from the cytoplasm and specific intracellular organelles. Many low-molecular-weight proteins including the cytokine interleukin-1β, alarmins, and lysosomal-cargo proteins exit cells in the absence of cell lysis. Cytokines and alarmins are released in an endoplasmic reticulum (ER)-Golgi-dependent manner as free proteins rather than by extracellular vesicles. Our work provides an experimental framework for the dissection of cellular exit pathways and a resource for pyroptotic protein release.

INTRODUCTION

Secreted proteins such as cytokines, chemokines, and growth factors have various functions in the initiation and resolution of inflammation and the regulation of effector cells (Arango Duque and Descoteaux, 2014). A major pathway contributing to protein secretion in macrophages involves a highly pro-inflammatory form of cell death, known as pyroptosis. Pyroptosis plays a central role in the regulation of immune responses during infection and tissue injury (Bergsbaken et al., 2009). Efficient execution of pyroptosis requires the activation of intracellular signaling complexes termed inflammasomes and is regulated tightly in two steps.

Inflammasomes are comprised of activated cytosolic receptors such as certain nucleotide-binding oligomerization domain-like receptors (NLRs), an adaptor protein ASC, and a downstream effector protease known as Caspase-1.

For activation, a first signal induces transcription and expression of some inflammasome proteins such as the NLR family pyrin domain containing protein 3 (NLRP3), whereas some other NLRs such as NLRP1 are expressed constitutively. *In vitro*, this "priming" signal is commonly provided by ligation of innate immune receptors such as Toll-like receptor 4 (TLR4) through the Gram-negative bacterial cell membrane component lipopolysaccharide (LPS) (Broz and Dixit, 2016). LPS also induces numerous cytokines and chemokines including interleukin 1 beta (IL-1β), tumor necrosis factor alpha (TNF-α), and C-X-C motif chemokine ligand 10 (CXCL10), of which most are directly released conventionally through the endoplasmic reticulum (ER)-Golgi secretory pathway (Kaisho and Akira, 2000; Stow et al., 2009).

A second signal triggers inflammasome assembly through the activation of NLRs. Low cytosolic potassium levels activate NLRP3, whereas removal of the N terminus activates NLRP1 (Mitchell et al., 2019; Swanson et al., 2019). NLRs can then recruit the adaptor protein ASC and activate pro-inflammatory caspases such as caspase-1 that cleaves its substrates IL-1β, IL-18, and the gasdermin protein family member Gasdermin-D (GSDMD) into biologically active forms. The N-terminal fragment of GSDMD forms pores in the plasma membrane (PM) and eventually causes cell lysis (Ding et al., 2016; Kayagaki et al., 2015; Liu et al., 2016). GSDMD thereby facilitates the release of proteins lacking a signal peptide such as the cytokines IL-1β and IL-18 and proteins or "alarmins" derived from damaged cellular organelles such as high mobility group box 1 protein HMGB1, which also exhibits paracrine activity (Evavold et al., 2018; Heilig et al., 2018; Lamkanfi et al., 2010). As this protein export pathway does not involve active protein transport through the secretory pathway, it is broadly referred to as "unconventional secretion"

(Lopez-Castejon and Brough, 2011; Ng and Tang, 2016; Nickel and Rabouille, 2009).

Proteins released during inflammasome-activated pyroptosis therefore comprise conventionally (e.g., TNF-α), and unconventionally (e.g., IL-1β) released cytokines as well as alarmins (e.g., HMGB1) and other proteins leaking from the cytosol and damaged intracellular organelles. Unlike conventionally secreted proteins, which can be computationally predicted based on the primary amino acid sequence of their signal peptide, unconventionally released proteins can be identified with high confidence only experimentally by assessment of their release and the accompanied accumulation in cellular supernatants (Nickel and Rabouille, 2009). As IL-1- and IL-18-independent effects of inflammasome-mediated inflammatory programs have been described in different pathologies, the presence of novel immunomodulatory proteins such as alarmins can be hypothesized to be released during pyroptosis (Gong et al., 2020; Lammert et al., 2020).

In addition to translocation through GSDMD pores or cell lysis, various other export mechanisms have also been implicated in unconventional secretion such as secretion by lysosomes, extracellular vesicles (EVs), autophagosomes, and PM-derived microvesicles (Andrei et al., 1999; Baroja-Mazo et al., 2019; Brough et al., 2017; Dupont et al., 2011; Lopez-Castejon and Brough, 2011; Martín-Sánchez et al., 2016; Monteleone et al., 2015; Rubartelli et al., 1990; Tapia et al., 2019; Zhang et al., 2015). The identification of the predominant mechanisms of release for each protein can therefore enable the development of strategies to specifically interfere with distinct export pathways by abrogating the release of defined sets of proteins and thereby altering responses of neighboring cells or the entire organism to pyroptosis.

Mass spectrometry (MS)-based proteomics has matured remarkably over the last years and now provides a powerful set of tools for the systematic and unsupervised examinations of cellular processes (Aebersold and Mann, 2016; Larance and Lamond, 2015). Building on our recently developed MS-based approaches for the comprehensive analysis of intercellular immune signals, we set out to devise an experimental strategy to determine the inflammatory program of pyroptotic macrophages in its entirety and define the exit route for each protein (Meissner et al., 2013; Rieckmann et al., 2017; Tanzer et al., 2020). Our strategy comprises genetic knockouts (KOs) and knockins of inflammasome proteins to specifically inhibit or provide only one of the two signals required for full inflammasome activation. We pharmacologically interfere with ER-Golgi protein transport or passive cell lysis and assess the contribution of membrane-enclosed vesicles and receptor shedding to pyroptotic protein release, with the latter having implications in necroptosis—a distinct form of inflammatory cell death (Cai et al., 2016; Tanzer et al., 2020). Thereby, we determine for each protein whether transcription, caspase activation, active secretion, organellar damage, pore formation, or passive cell lysis is required for its release during pyroptosis.

RESULTS

Quantitative proteomics accurately determines protein release

We activated conventional protein secretion through one signal (TLR4 with LPS) and unconventional secretion through two signals (TLR4 with LPS plus NLRP3 with ATP or Nigericin) in murine bone-marrow-derived and human-monocyte-derived macrophages (BMDMs and HMDMs, respectively) and analyzed the secretory programs by label-free, high-resolution MS in a single-shot liquid chromatography-tandem MS (LC-MS/MS) format by using a Quadrupole-Orbitrap instrument (Figures 1A, S1A, and S1B; Kelstrup et al., 2018; Scheltema et al., 2014). Fold changes of proteins released in mouse and human macrophages upon TLR4 or TLR4 plus NLRP3 activation compared to untreated controls are indicated in Table S1. We identified on average almost 3,000 protein groups in cellular supernatants at a peptide and protein false discovery rate (FDR) of 1% (Figures S2A and 2B). We compared MS- to antibody-based (ELISA) protein quantification using TNF-α and IL-1β as reference proteins for conventional and unconventional secretion pathways (Figures 1B–1G and S2G). Both quantification methods showed similar secretion profiles for the two proteins (Figures 1B–1G), with an average correlation of 0.7 for TNF-α (Figure S2G) and 0.95 for IL-1β (Figure S2G). As expected, TNF-α was secreted after TLR4 activation regardless of the presence of a second activation signal (Figures 1B and 1E). In contrast, IL-1β was only secreted after priming the cells through TLR4, followed by activation of NLRP3 (Figures 1C and 1F). We further determined cell death by lactate dehydrogenase (LDH) release (Figure 1D) as well as by the summed MS signal of all proteins annotated as cytosolic (Figure 1G) and obtained a correlation of 0.85 between the two methods (Figure S2G). Our analysis shows that our method accurately quantifies conventional and unconventional protein secretion as well as cell death in activated macrophages.

Kinetics of conventional and unconventional protein release

To define pyroptotically released proteins, we assigned proteins to either (1) conventionally secreted or (2) unconventionally secreted proteins by comparing kinetics of secretomes from different experimental conditions (Figure 1).

First, we defined conventionally secreted proteins by comparing the secretome of TLR4-activated cells to unstimulated cells (Figure 1H). We identified 36 significantly released proteins, of which 30 exhibit a signal peptide and signal anchor. Among these proteins are known conventionally secreted, inflammatory mediators including cytokines (e.g., TNF-α and IL-6) and chemokines (e.g., CXCL10), confirming results of published work (Meissner et al., 2013). Functional enrichment analysis using annotations from the UniProt Keywords database revealed common terms of conventionally released inflammatory mediators such as "Cytokine," and "Inflammatory response" (Figure S3A).

Second, we defined unconventionally secreted proteins by the combined activation of TLR4 and NLRP3. Under these conditions, cellular supernatants contain conventionally secreted proteins due to the TLR4 priming signal and unconventionally released proteins comprising of proteins released by GSDMD pores or due to cell lysis (Figure 1I). This group of proteins contained prototypic unconventionally secreted proteins such as IL-1β, IL-1α, IL-18, and HMGB1 but excluded prototypic conventionally exported proteins like TNF-α and Cxcl10 (Figure 1I). Enrichment analysis of unconventionally secreted proteins using UniProt Keywords and Pfam protein domains unveiled the presence of diverse protein classes

CellPress
OPEN ACCESS

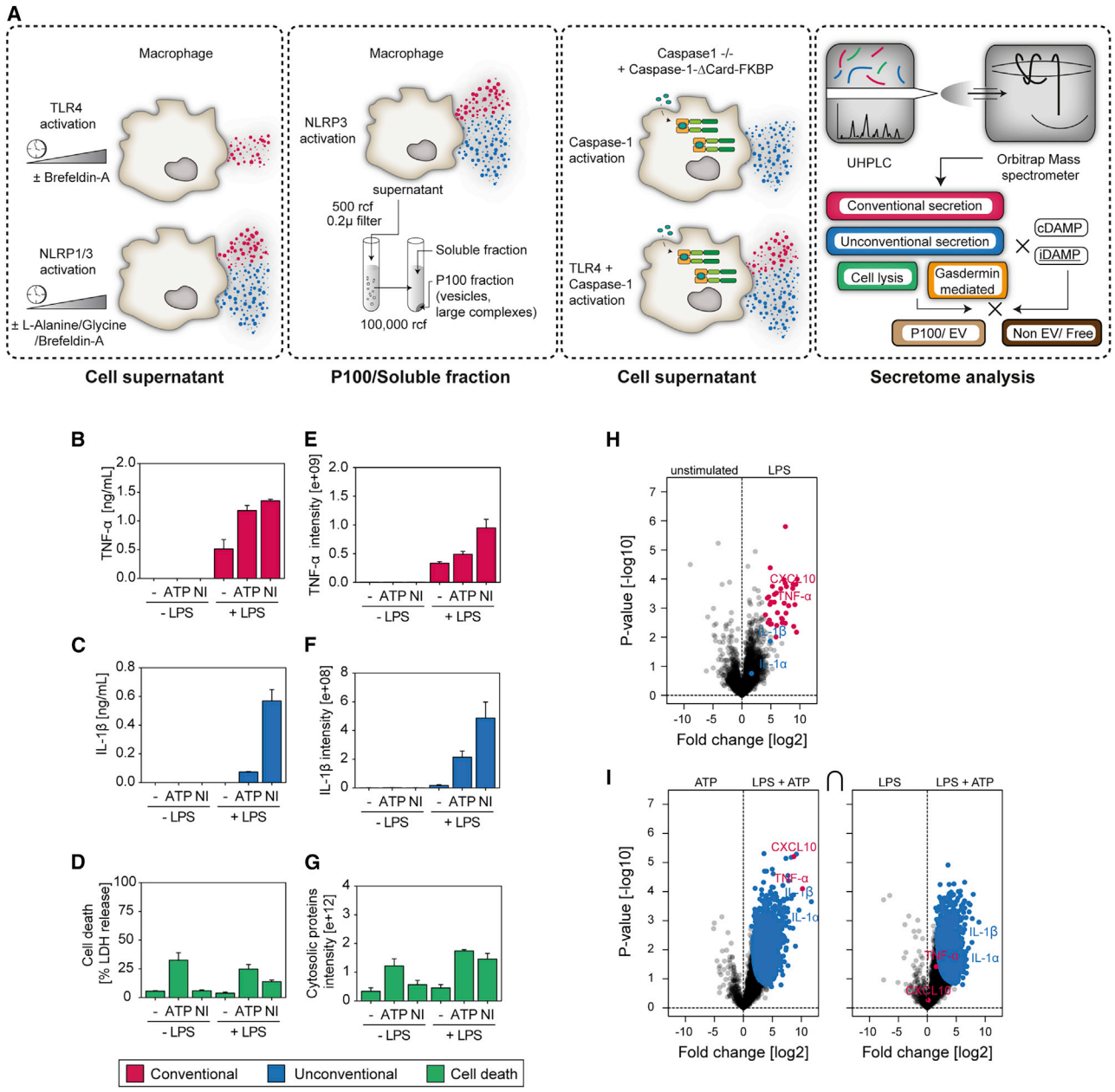

Figure 1. Quantitative proteomics workflow to identify proteins released by macrophage pyroptosis

(A) Schematic illustration of the experimental approach to distinguish between different modalities of protein release from cells, including conventional, unconventional, cell lysis dependent and independent, soluble or extracellular vesicle associated, dissection of released induced or constitutive alarmins, or damage-associated molecular patterns (DAMPs). Workflow consisting of macrophage activation, collection and processing of supernatants, sample preparation, LC-MS/MS analysis, and data processing.

(B–D) Quantification of TNF-α (B) and IL-1β (C) secretion by ELISA or cell death by LDH release (D) after TLR4 and NLRP3 activation in mouse macrophages. Data are represented as mean ± SD of three biological replicates.

(E–G) MS raw intensity-based quantification after TLR4 and NLRP3 activation in mouse macrophages of TNF-α (E) and IL-1β (F) secretion and cell death (G) measured by the summed MS raw intensity of all proteins annotated as "cytoplasm," "cytoplasmic part," "intracellular," or "intracellular part" by GOCC. Data are represented as mean ± SD of three biological replicates.

(H and I) Volcano plots showing secreted proteins from differentially activated BMDMs. Pairwise secretome comparisons to define conventionally (H) and unconventionally (I) released proteins. (H) Conventionally released proteins upon TLR4 activation compared to untreated controls (magenta).

(I) Unconventionally released proteins upon TLR4 plus NLRP3 compared to TLR4 as well as to only NLRP3-activated cells (blue). Significant proteins were determined with a parametric two-tailed Welch's t test (FDR < 0.05, $S_0 = 1$).

See also Figures S1–S4 and Table S1.

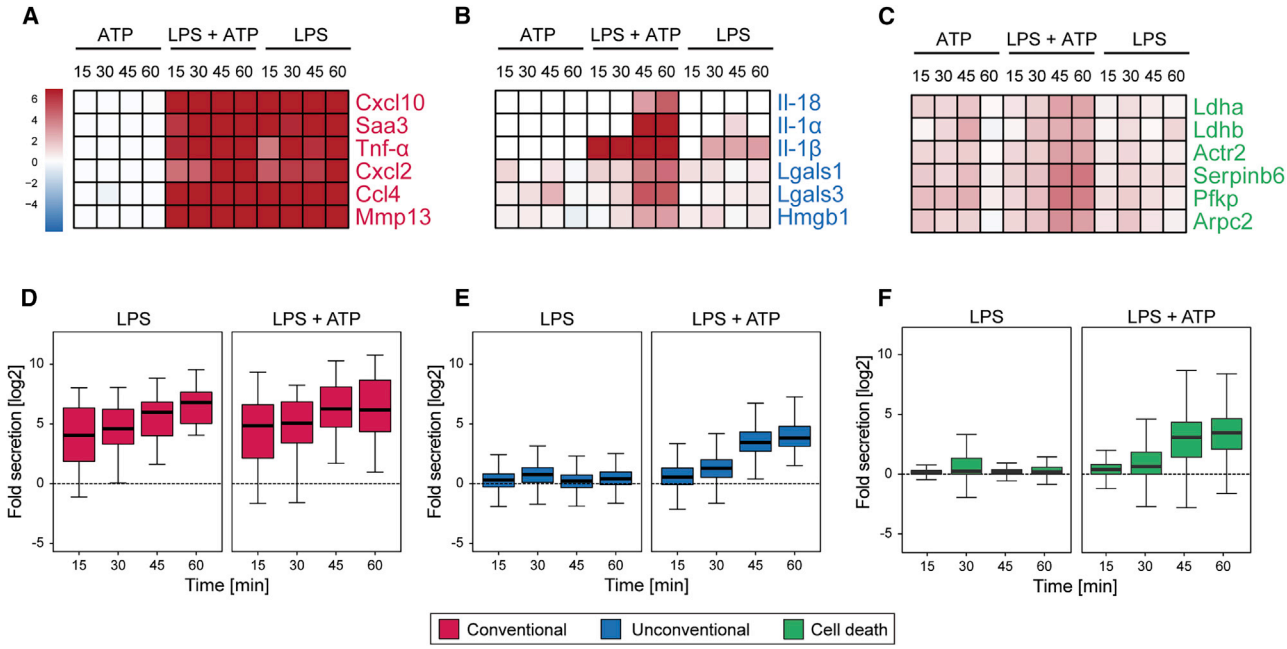

Figure 2. Proteomic analysis of pyroptosis-mediated conventional and unconventional protein secretion

(A–C) Heatmaps with secretion profiles of selected proteins known to be released via conventional unconventional programs.

(A) Cytokines containing a signal peptide and significantly released from cells by conventional secretion upon TLR4 activation with LPS.

(B) Cytokines/alarmins without a signal peptide significantly released from cells by unconventional secretion upon pyroptosis induction by TLR4 and NLRP3 activation with LPS and ATP.

(C) Selected cytoplasmic proteins, including subunits of the LDH complex.

(D–F) Fold secretion over time of conventional (D; magenta), unconventional (E; blue), or proteins annotated as "cytoplasm," "cytoplasmic part," "intracellular," or "intracellular part" by GOCC (F; green) by BMDMs activated for TLR4 with LPS and TLR4 plus ATP for NLRP3.

See also Figures S1, S2, and S4 and Table S1.

and structural domains such as Cofilin-actin de-polymerization factor (Cofilin-ADF) and Lin11, Isl-1 & Mec-3 (LIM), ADP ribosylation factor (ARF), and the caspase activation and recruitment domain (CARD), which is present for example in caspase-1 and ASC, two proteins involved in the formation of the NLRP3 inflammasome (Figure S3B). The abundance of conventionally secreted proteins increased gradually over time in response to TLR4 activation (Figures 2A and 2D), whereas unconventional protein release increased steadily in response only to TLR4 plus NLRP3 and was detectable already at 15 min after activation with a peak at 45–60 min (Figures 2B and 2E). We detected IL-1 release early upon inflammasome activation at 15 min, whereas other pyroptotically released cytokines and damage-associated molecular patterns (DAMPs) like IL-18 and HMGB1, respectively, with a similar size as IL-1β peaked later at 30–45 min (Figures 2B and 2E; Table S1).

Inhibition of NLRP3 with its small-molecule antagonist glyburide or KO of the downstream effector Caspase-1 abrogated the unconventional secretion completely (Figures S3D, S3E, and S4A–S4C; Swanson et al., 2019). Despite multiple comparisons, thousands of proteins were identified to be released with similar kinetics to IL1 and IL-18, impairing the discovery of potential novel alarmins. We therefore set out to define protein release pathways by assessing the role of the ER-Golgi compartment, extracellular vesicles, damaged intracellular organelles, PM pores, or cell lysis during pyroptosis.

The ER-Golgi compartment is required for inflammasome formation and unconventional protein release

Although the role of the ER-Golgi route conventional secretion has been well described, its contribution to unconventionally released cytokines such as IL-1β remains controversial and incompletely understood (Rubartelli et al., 1990; Zhang et al., 2017). We used the fungal metabolite Brefeldin A (BFA) as well as the small molecule Golgicide A (GCA), of which both prevent protein transport from the ER to the Golgi and disrupt the function of ER-Golgi secretory pathway (Chardin and McCormick, 1999; Sáenz et al., 2009). BFA and GCA perturb ER-Golgi trafficking by specifically inhibiting the guanine nucleotide exchange factors (GEFs) that regulate the formation of secretory vesicles. Although BFA targets several GEFs, including Golgi-specific BFA resistance factor 1 (GBF1), BFA-inhibited GEF 1 (BIG1), and BIG2, GCA is highly specific toward GBF1 (Sáenz et al., 2009). As expected, treatment of LPS-stimulated BMDMs with BFA inhibited the secretion of TNF-α and all other proteins we defined as conventionally secreted in a dose-dependent manner (Figures 3A and 3D). BFA also inhibited NLRP3-mediated release of IL-1β and cell death (Figures 3B, 3C, and 3E), in keeping with previous reports with a similar dose dependency (Zhang et al., 2017). However, we also observed a substantial reduction in IL-1β secretion by BFA treatment for inflammasome sensors, including baculoviral inhibitor of apoptosis domain repeat-

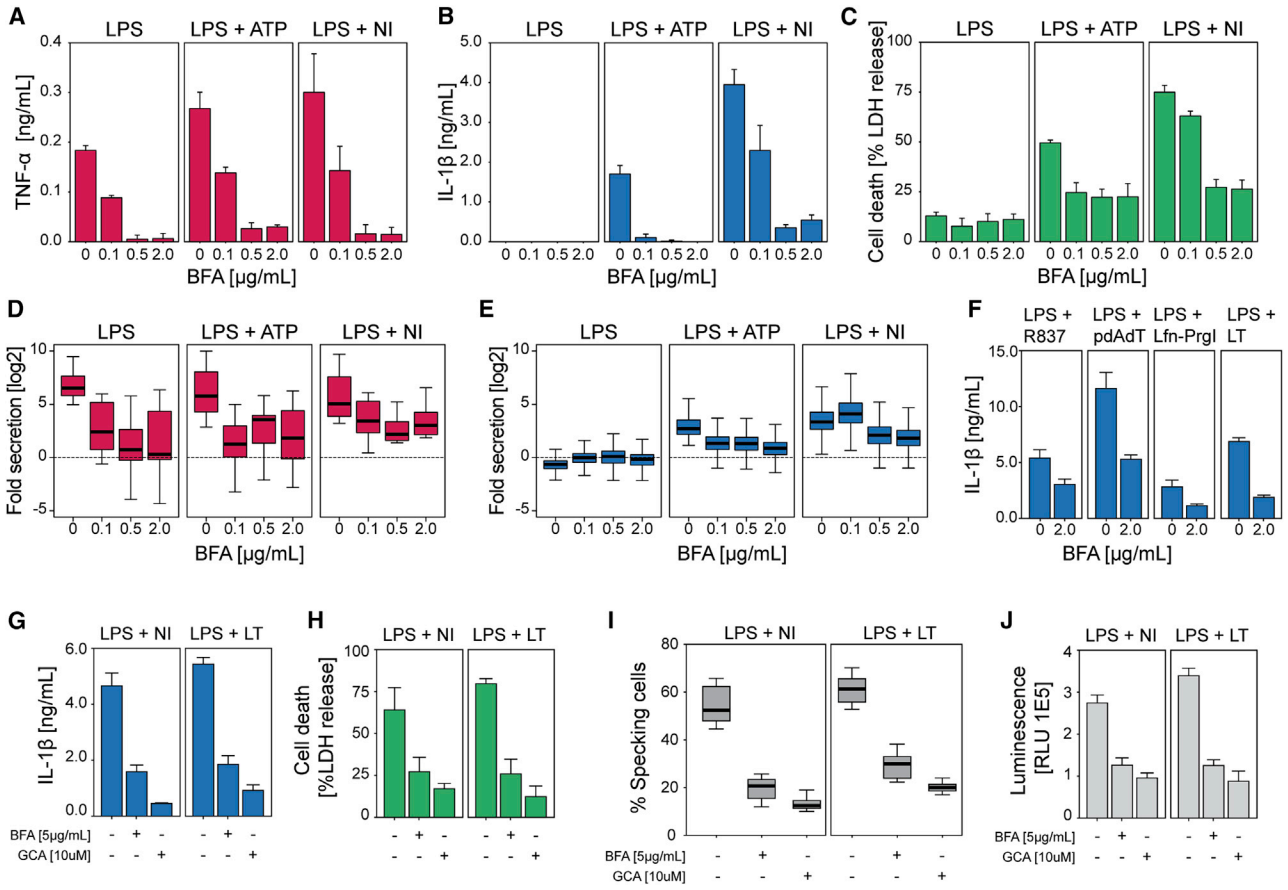

Figure 3. Conventional secretion, inflammasome formation, and unconventional secretion are inhibited by pharmacological ER-Golgi disruption

(A–C) ELISA of TNF-α (A), IL-1β (B), and LDH released (C) in supernatants of TLR4- or NLRP3-activated BMDMs in the presence of the indicated concentrations of BFA. NI, Nigericin

(D and E) Fold secretion of conventionally (D; magenta) and unconventionally (E; blue) released proteins in TLR4- and TLR4 plus NLRP3-activated BMDMs in the presence of the indicated concentrations of BFA.

(F) IL-1β levels as determined by ELISA in supernatants of NLRP3-, AIM2-NLRC4-, and NLRP1-activated BMDMs in the presence of the indicated concentrations of BFA.

(G–H) IL-1β levels as determined by ELISA (G) and LDH release (H) in supernatants of NLRP3- and NLRP1-activated BMDMs in the presence of the indicated concentrations of BFA or GCA.

(I–J) Quantification of NLRP3 or NLRP1 inflammasome assembly in the presence or absence of the indicated concentrations or BFA or GCA by evaluating Asc speck formation by using fluorescent microscopy. Data are compiled from three biological replicates, each with 100–200 quantified cells.

(I) Measurement of Caspase-1 activity by luminescence, in which aminoluciferin generated by cleavage of its substrate Z-WEHD-aminoluciferin results in light production in the presence of the luciferase enzyme. Data are represented as mean ± SD of three biological replicates.

See also Figures S4 and S5 and Table S1.

containing protein 1 (NAIP1) activated with its ligand the bacterial type III secretion system component PrgI and absent in melanoma 2 protein (AIM2) activation with repetitive synthetic double-stranded DNA sequence of poly(dA-dT) (Figure 3F; Broz and Dixit, 2016). GCA induced a similar reduction in IL-1β secretion and cell death in BMDMs activated for both NLRP1 and NLRP3 (Figures 3G and 3H). Notably, we treated cells with BFA or GCA after the first priming signal, suggesting that inhibition occurs at the level of the inflammasome sensor or the execution of pyroptosis but not TLR4. Interestingly, both BFA and GCA substantially reduced Asc speck formation as well as Caspase-1 activation (Figures 3I, 3J, and S5A–S5C). Thus, our data show that ER-Golgi perturbation with BFA and GCA inhibits unconventional protein release by interfering with inflammasome formation, regardless of the tested inflammasome sensor.

Leakage of specific cellular organelles during pyroptosis

We next asked whether pyroptosis leads to the release of subcellular organelles and their contents into the extracellular environment. To assess the leakage of proteins from organelles, we inspected the subcellular origin of all significantly released proteins. We observed an enrichment of cytosolic and lysosomal proteins and, to a lesser degree, endosomal, mitochondrial,

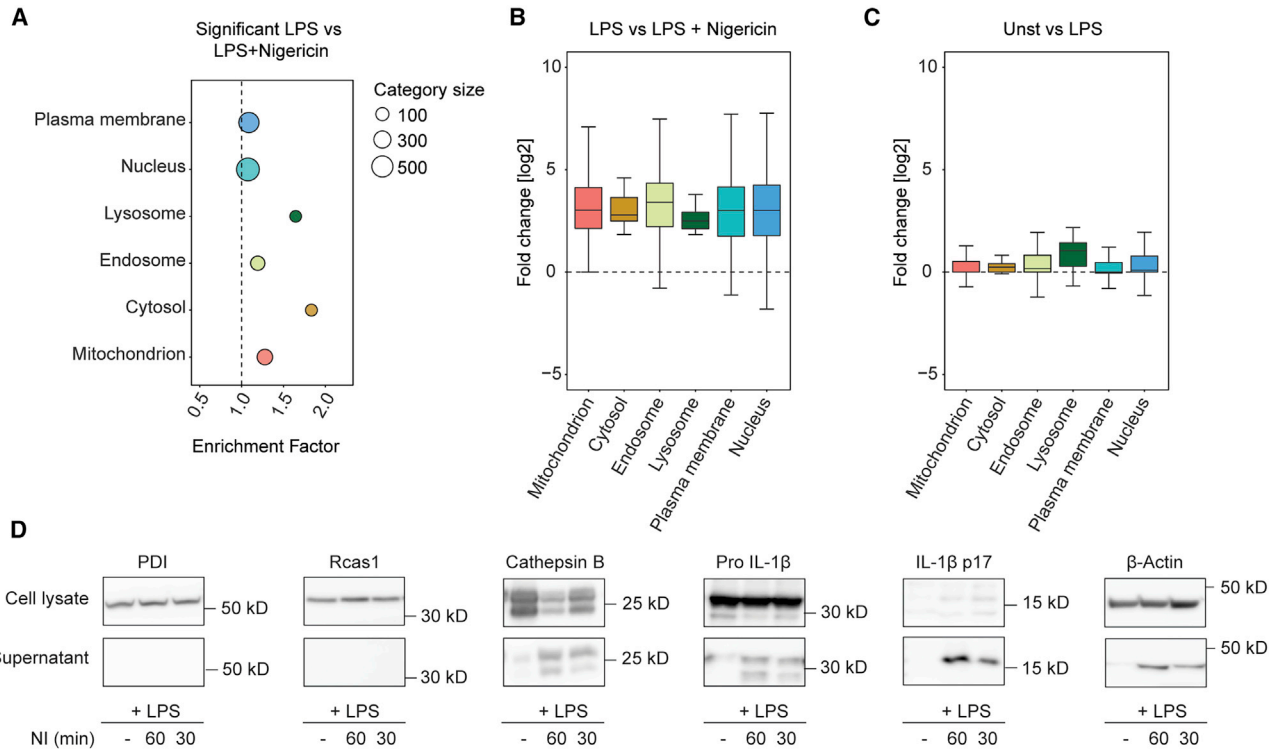

Figure 4. Extracellular leakage of organellar proteins

(A) Balloon plot of organelle marker enrichment analysis on the unconventional secretion signature after TLR4 and NLRP3 activation in mouse macrophages by using GOCC slim terms. Enrichment factors were calculated by Fisher's exact test (annotations with intersection sizes of >15 and $p < 0.002$ are shown). Category sizes are represented by balloon size.

(B and C) Boxplots indicating the fold changes of all detected proteins belonging to indicated organelles in the unconventional (B) and conventional (C) secretomes.

(D) Western blots of cell lysates or supernatants after TLR4 or TLR4 and NLRP3 activation for ER, Golgi, and lysosomal markers PDI, Rcas1, and Cathepsin B, respectively; or pro IL-1β, IL-1β p17 fragment, and the housekeeping protein β-Actin. Immunoblotting data are representative of two biological replicates.

See also Figure S3.

nuclear, and PM proteins (Figures 4A and 4B). Interestingly, proteins from the ER and Golgi were not enriched. In agreement with our MS analysis, immunoblotting confirmed the release of the luminal lysosomal marker Cathepsin B and the absence of ER lumen marker protein disulfide isomerase (PDI) and Golgi marker receptor binding cancer antigen expressed on SiSo cells (RCAS1) in pyroptotic supernatants (Figure 4D). Our analysis therefore suggests that pyroptosis induces the release of proteins from specific subcellular localizations into the extracellular environment, whereas other organelles are retained inside the cell corpse.

We and others have described the shedding of receptors during programmed cell death by necroptosis (Tanzer et al., 2020). To determine whether pyroptosis is also accompanied by receptor shedding, we assessed whether cell surface receptors are enriched in pyroptotic cell supernatants. We detected 62 receptors, of which 15 were significantly released. However, examination of the quantified peptides revealed that both cytoplasmic and extracellular domains of these receptors were released to a comparable extent (Figure S5A). These results suggest the absence of an active shedding process involving proteolytic cleavage of receptors, as this would be accompanied by an increase of the extracellular domains of receptors and not the corresponding cytoplasmic domain. We therefore surmise that the presence of receptors and other PM-localized proteins in pyroptotic supernatants can be ascribed primarily to the release of PM fragments or micro-vesicles.

Most cytokines are secreted in a soluble form and not in EVs

EVs have been implicated in programmed cell death and also in NLRP3-mediated release of both pro-form and mature IL-1β and IL-18 (Cypryk et al., 2018). To determine the contribution of this protein release route, we enriched EVs from LPS-activated or pyroptotic supernatants by using differential centrifugation as described previously (Lobb et al., 2015; Table S1). The majority of cytokines including IL-1β and IL-18 were not detected in the EV-enriched P100 fraction, indicating that they are predominantly secreted in a non-EV-bound, soluble form (Figures 5A–5C). Some cytokines like TNF-α and PF4 as well alarmins like HMGB1 were, however, also present in the P100 fraction, suggesting that they might be released in soluble forms as well as in membrane-associated or EV-incorporated forms (Figure 5B). As both, low- and high-abundant cytokines were equally

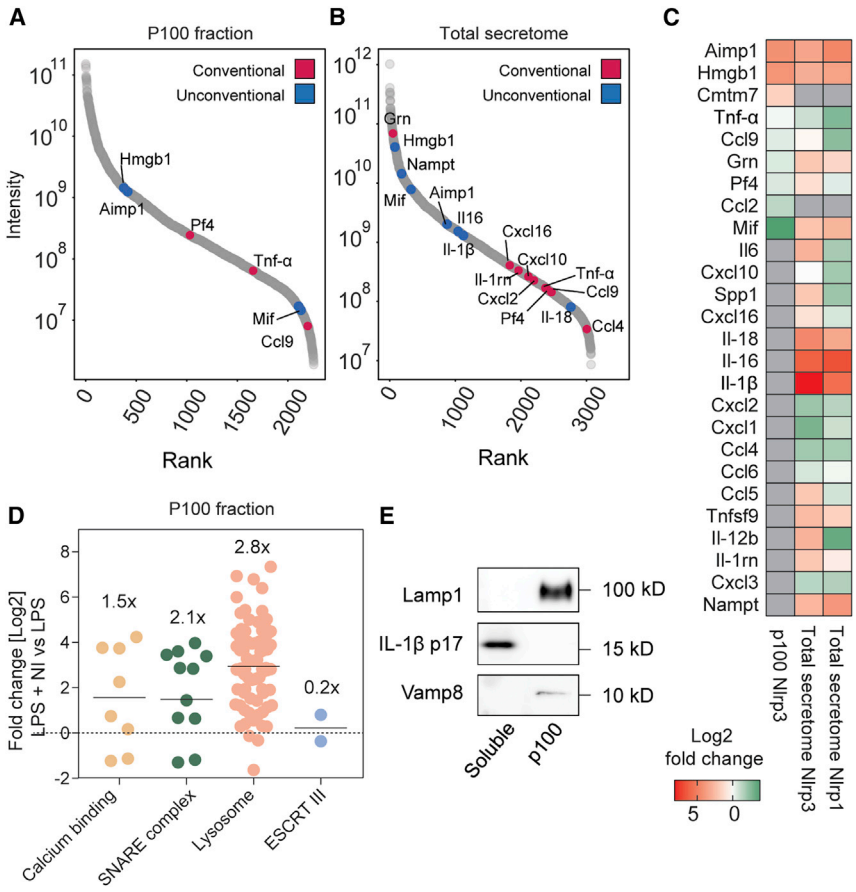

Figure 5. Majority of cytokines are released as free proteins and not in EVs

(A and B) Intensity-based ranking of cytokines identified in either P100 (A) or total secretome (B) of NLRP3-activated murine macrophages.

(C) Heatmap of fold secretion of conventionally and unconventionally released cytokines by murine macrophages in the total secretome after NLRP1/3 activation or P100/EV-associated secretome after NLRP3 activation.

(C) Swarm plots showing log2 fold change of proteins assigned to the annotation "Calcium/phospholipid binding," "SNARE complex," "Lysosome" and "ESCRTIII complex" present in P100/EV fraction of pyroptotic cells compared with TLR4-activated controls.

(D) Presence of lysosomal marker Lamp1, IL-1β p17 fragment, and the SNARE complex member Vamp8 in either the soluble or P100 fraction after NLRP3 activation evaluated by immunoblotting.

See also Figures S1, S3, and S6 and Table S1.

detected in the P100 fraction, our analysis is not biased toward the detection of high-abundant cytokines (Figure 5B). We conclude that secretory processes, in which cytokines and alarmins are packaged into vesicles and released in such a membrane-encapsulated form, contribute only minimally to their release during pyroptosis.

We also observed an enrichment of proteins in the categories "Lysosome," "SNARE complex," and "Calcium/PI binding," which we had also detected previously in vesicles released by cells undergoing necroptosis—another form of lytic cell death (Figure 5D; Tanzer et al., 2020). Both membrane as well as luminal lysosomal proteins were enriched to a comparable degree in the P100 fraction and secretome (Figure S3F). Conversely, cytosolic proteins were largely depleted in this fraction (Figures 5B–5D). Our data therefore suggest that endosomal and lysosomal proteins are released in a vesicular form during pyroptosis. We confirmed the absence of IL-1β or the presence of the lysosomal marker LAMP1 and SNARE complex member VAMP8 in the P100 fraction by immunoblotting (Figure 5E).

Unconventional release of low-MW, lysosomal, and mitochondrial proteins proceeds by a GSDMD-mediated but cell-lysis-independent pathway

Multiple recent studies indicate that during pyroptosis, low-molecular-weight (MW) proteins including IL-1β are released through PM GSDMD pores independently of late-stage cell lysis (DiPeso et al., 2017; Evavold et al., 2018; Heilig et al., 2018). To assess the contribution of GSMDM pores versus cell lysis to protein release, we induced pyroptosis in the presence of osmoprotectants L-alanine or glycine, which have been shown to block cell lysis but not the formation of GSDMD pores (Fink and Cookson, 2006; Loomis et al., 2019). Both L-alanine and glycine inhibited cell lysis that was measured by the release of the LDH complex of approximately 147 kD but not IL-1β (17 kD) or any conventionally secreted cytokine like TNF-α (26 kD), in keeping with previous reports (Figure S4D). We further evaluated protein release in GSDMD KO iBMDMs or wild-type (WT) BMDMs treated with the GSDMD inhibitor necrosulfonamide A (NSA), confirming that cell lysis as well as IL-1β release was inhibited, whereas conventional secretion of TNF-α was not (Figures S4E and S4F; Evavold et al., 2018; Heilig et al., 2018; Rathkey et al., 2018). At the global level, the correlation between all proteins released unconventionally versus the subset released in an osmoprotection-independent manner was mediocre (0.36) (Figures 6A–6C), whereas conventionally versus unconventionally released proteins showed a negative correlation (−0.16), indicating the independence of these two protein export pathways (Figures 6B and 6C).

Our proteomics experiments reveal that sensitivity to osmoprotection depends on the MW of a protein, as the release of low-MW proteins was inhibited far less than high-MW proteins (Figure 6D; Table S1). Osmoprotection barely reduced the release of low-MW proteins. such as IL-1β, the alarmins Galectin 3 (LGALS3) and HMGB1, or cytosolic proteins such as glutaredoxin 5 (GLRX5), whereas GSDMD KO or inhibition completely blocked the release of low- as well as high-MW proteins (Figures 6E and 6F). Surprisingly, a Gene Ontology term cellular component (GOCC) enrichment analysis revealed that proteins derived from lysosomes and, to a lesser extent, from mitochondria

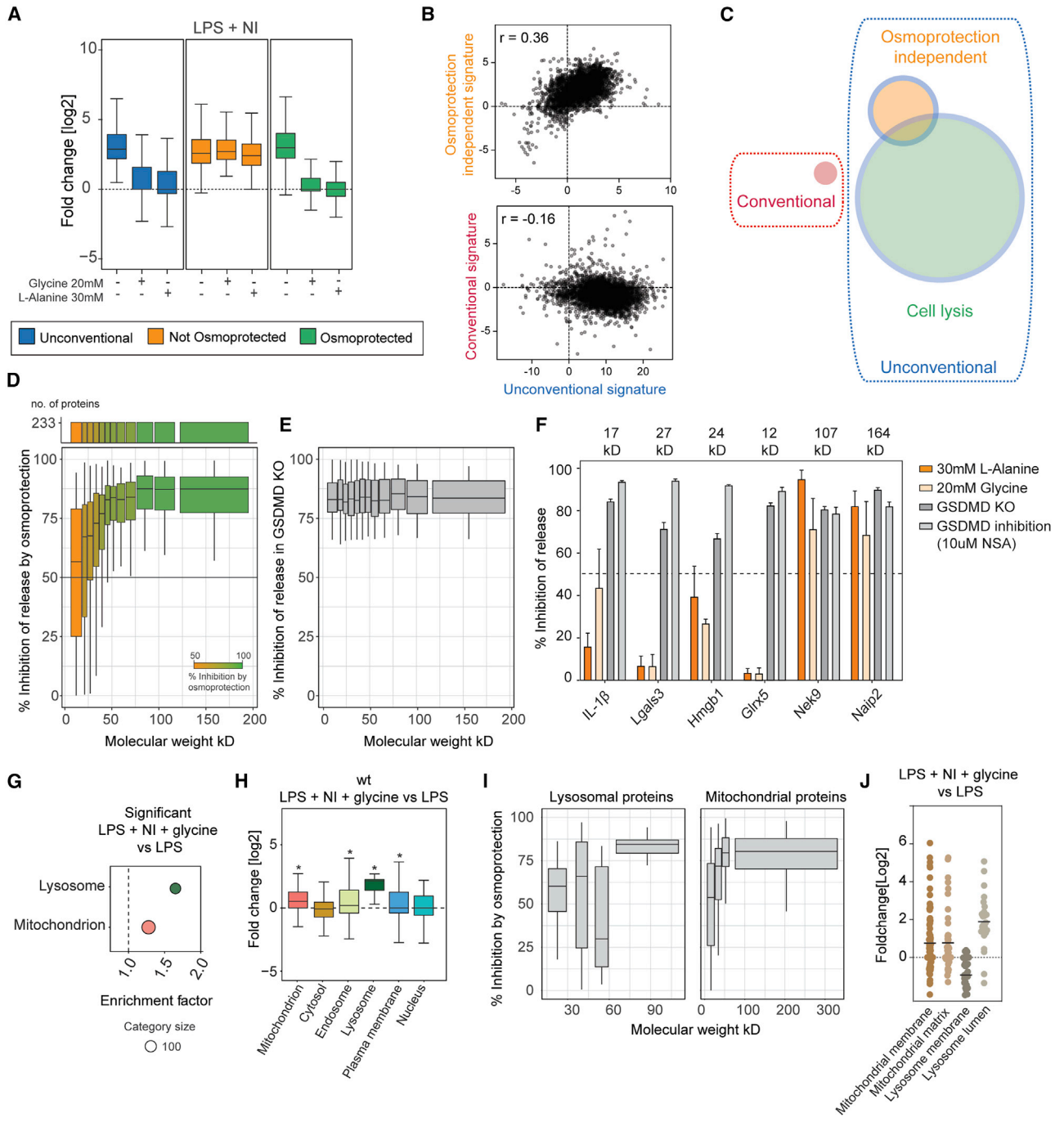

Figure 6. Release of low-MW, mitochondrial, and lysosomal proteins is dependent on GSDMD but proceeds independently of cell lysis

(A) Fold secretion of all unconventional, osmoprotection-independent (orange), and cell-lysis-dependent (green) protein release in TLR4 plus NLRP3-activated BMDMs in the presence of the indicated concentrations of L-Alanine or Glycine.

(B) Correlations of t test differences used to define the conventional, unconventional, osmoprotection, or cell lysis-independent and -dependent signatures. Conventional signature, LPS versus unstimulated; unconventional signature, t test differences LPS + NI versus LPS; and osmoprotection/cell lysis independent, LPS + NI + 30 mM L-alanine/20 mM glycine versus LPS.

(C) Venn diagram of proteins released conventionally, unconventionally, and osmoprotection independently or passively by cell death.

(D–F) Effect of osmoprotection or knockout of GSDMD on unconventionally released proteins with different MWs. Boxplot indicating the extent of inhibition by osmoprotection (D) or GSDMD knockout (E) to unconventionally released proteins binned according to increasing MW. Number of proteins per bin are indicated. Bar plots of selected proteins indicate the degree of inhibition of their release by osmoprotection, GSDMD knockout, or inhibition by NSA (F).

(legend continued on next page)

contribute to the osmoprotection-independent protein release (Figures 6G and 6H). Further analyses revealed that only lysosomal lumen but not membrane proteins are released independent of their MW, presumably as vesicular cargo (Figures 6I and 6J). In contrast, we detected both mitochondrial matrix and mitochondrial membrane proteins, which are sensitive to osmoprotection depending on their MW, arguing against a significant contribution of released mitochondrial vesicles under these conditions (Figure 6J). We therefore conclude that a GSDMD-dependent, cell-lysis-independent pathway facilitates the release of many constitutively expressed small-MW proteins derived from the cytoplasm and other cellular organelles, for which extracellular functions have not been described yet.

The majority of pyroptotically released alarmins do not require induction

As the two-step activation comprising priming and NLR activation executes a convoluted secretory program, we considered experimental systems, in which a single trigger is sufficient for inflammasome activation. Caspase 1/11 double knockout (DKO) iBMDMs reconstituted with Caspase-1 fused to the FK506 binding protein (FKBP) dimerization domain (Casp1ΔCard-FKBP) provides an elegant solution, as Caspase1 can be dimerized and activated by AP20187, leading to pyroptosis (MacCorkle et al., 1998; Rühl et al., 2018). Notably, activation of Caspase-1 is independent of priming and thereby enables the dissection of proteins released with and without priming. As expected, IL-1β is released only upon priming and AP20187 treatment, whereas conventional secretion, for example of TNF-α, requires priming but is unaffected by AP20187 (Figures 7A and 7B). Cell death, however, is executed only upon addition of AP20187, independent of priming (Figure 7C). This experimental setup therefore enables the distinction of two classes of proteins—constitutive and induced damage-associated molecular patterns (c- or iDAMPs) (Yatim et al., 2017). The release of the majority of unconventionally released proteins occurs irrespective of priming (Figure 7D). The alarmin HMGB1 is one such protein and can therefore be classified as a cDAMP. Our proteomic investigations reveal that pyroptotic cell death serves as an exit route also for other cDAMPs, such as macrophage migration inhibitory factor (MIF), mminoacyl TRNA Synthetase Complex Interacting Multifunctional Protein 1 (AIMP1), galectins, and S100 families (Figure 7D; Table S1). We confirmed the release of MIF and AIMP1 by ELISA and immunoblot analysis (Figures 7G and 7H). As most cDAMPs, such as MIF or LGALS 1, 3, and 9, have a low MW, they are released independently of cell lysis, whereas others, such as AIMP1 or nicotinamide phosphoribosyltransferase (NAMPT), are predominantly released due to cell lysis. The cellular mechanisms regulating the exit of major protein classes are shown in Figure 7I and Table S1.

In contrast, IL-1β is released only during pyroptosis after priming and therefore is a paradigm iDAMP (Figure 7E). IL-18 shares some features of both classes, and even though priming boosts its expression and release, a smaller amount is constitutively expressed and therefore released independently of priming (Figures 7E and 7F; Marshall et al., 1999). Our analysis reveals that IL-1β is unique in its regulation and release kinetics, as it is among the top 5 most highly induced proteins upon priming and thereby differs from most other pyroptotically released proteins. (Figure S7A). The majority of strongly induced proteins include conventionally released cytokines that do not require pyroptosis for release (Figure S7B). Only a handful of other proteins not associated with extracellular functions, such as NLRP3, a few Ifit protein family members, and Oasl and Gbp family proteins, require priming for their induction and release by pyroptosis.

According to our global analysis, the cytokines IL-1β and IL-18 are unique in terms of their regulation in multiple steps, such as priming, proteolytic activation, MW, and PM-pore-mediated release. We did not detect any other proteins requiring a comparable complex regulation for release. This underscores the tight regulation of IL-1β and IL-18 activity, as they require hours to unfold their powerful inflammatory potential on neighboring cells or the whole organism. In contrast, a low MW and PM pore formation are sufficient for the release of most alarmins, which can be quickly released into the extracellular space and activate neighboring cells in a matter of minutes.

DISCUSSION

Activated macrophages control immune responses by releasing proteins, such as pro-inflammatory cytokines and alarmins. Variations in the secretory composition results in vastly different physiological responses of neighboring cells and the whole organism (Arango Duque and Descoteaux, 2014). We developed a generic and unbiased secretomics strategy based on pharmacological, genetic, and biochemical dissection of cellular protein release pathways. We applied it to analyze complex proinflammatory programs in macrophages upon activation of the following two major pathways of protein release: TLR4 activation and inflammasome-mediated pyroptotic cell death.

In addition to known cytokines and alarmins, we observed the unconventional release of thousands of proteins with diverse intracellular functions and localization during pyroptotic cell death. Our analytical framework facilitates the discovery of proteins released from sub-cellular organelles, including

(G) Organelle marker enrichment analysis of cell-lysis-independent unconventional release. Proteins significantly released upon NLRP3 activation in the presence of osmoprotection (LPS + NI + 30 mM L-alanine/20 mM glycine versus LPS) were defined to be cell lysis independent. Significant proteins were determined with a parametric two-tailed Welch's t test (FDR < 0.05, S_0 = 1). Enrichment factors were calculated by Fisher's exact test as described previously (annotations with intersection sizes of >15 and p < 0.002 are shown). Category sizes are represented by balloon size.
(H) Boxplots indicating the fold changes of all detected proteins belonging to indicated organelles in the unconventional secretomes in the presence of glycine.
(I) Effect of osmoprotection on mitochondrial and lysosomal proteins of different MWs. Boxplots indicating the extent of inhibition by osmoprotection to unconventionally released mitochondrial and lysosomal proteins binned according to increasing MW.
(J) Swarm plots showing log2 fold change of proteins assigned to the indicated annotation released during osmoprotection of pyroptotic cells compared with TLR4 activated controls.
See also Figure S4 and Table S1.

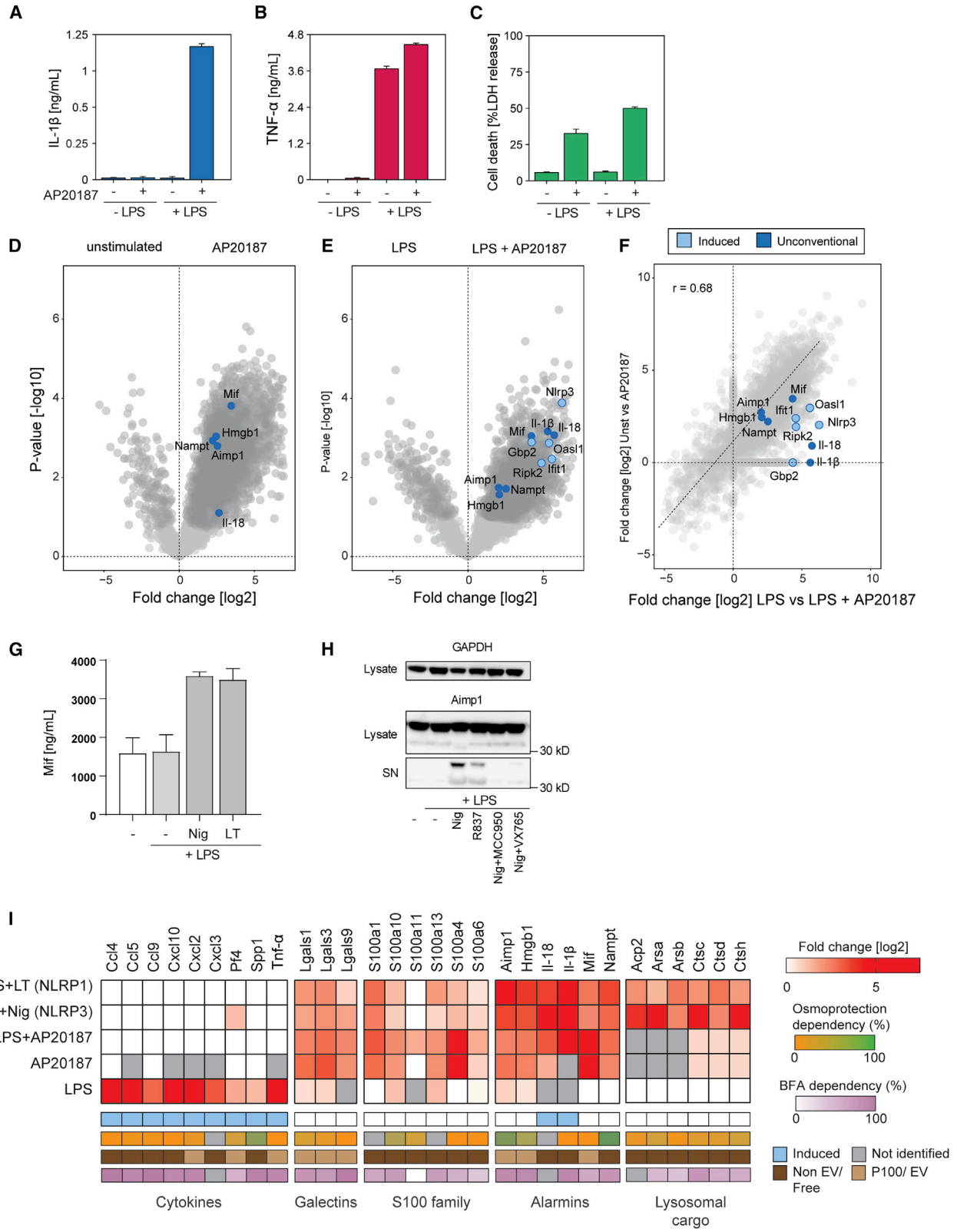

(legend on next page)

intracellular proteins with moonlighting or unexpected extracellular functions (Hernández et al., 2014; Jeffery, 1999). Conventional and unconventional secretory programs appear conserved across species based on the observed high correlation of mouse and human macrophage secretomes (Figure S4F).

We report that ER-Golgi disruption with BFA and GCA inhibits unconventional protein release and pyroptosis by interfering with inflammasome formation. Our data suggest that this effect is not only specific to NLRP3 as reported by Zhang et al. (2017) but also independent of the inflammasome sensor involved, although cell type and duration of BFA treatment affects cellular phenotypes. For example, IL-1β release was reported to be independent from the ER-Golgi compartment in LPS-treated human monocytes (Rubartelli et al., 1990). Moreover, long-term ER stress by BFA presumably activates the unconventional release of IL1β, whereas acute ER stress inhibits it (Bronner et al., 2015; Menu et al., 2012).

We show that EVs do not significantly contribute to cytokine and alarmin release during macrophage pyroptosis. It is interesting to speculate that incorporated or associated proteins might signal over longer durations and distances or upon intracellular release by membrane fusion with recipient cells.

We identified the presence of a large number of lysosomal cargo proteins, including many proteases, in the extracellular space during pyroptosis. Lysosomal proteases have been detected in the extracellular environment during various biological processes, including necroptosis and extensive TLR4 activation (Meissner et al., 2013; Mohamed and Sloane, 2006; Tanzer et al., 2020). Lysosomal exocytosis has been described as a membrane repair mechanism triggered by calcium influx (Bergsbaken et al., 2011; Tanzer et al., 2020). However, it remains unresolved how lysosomal content is released upon TLR4 activation in the absence of pore formation, PM damage, or cell death and whether this involves calcium fluxes. The presence of lysosomal proteases in the extracellular environment has been shown to play a role in tissue regeneration or tumor metastasis by remodeling the extracellular matrix (ECM) (Mohamed and Sloane, 2006; Olson and Joyce, 2015), and further studies should evaluate how these processes are affected by different forms of cell death.

Osmoprotection with the amino acids L-alanine and glycine has been described to delay pyroptotic cell lysis but not GSDMD pore formation in the PM. Under these conditions, protein release takes places through GSDMD pores only. Our data show that although cell lysis facilitates the unconventional release of the majority of proteins, the release of a subset of low-MW proteins, namely, cytokines/DAMPs including IL-1β, occurs independently of cell death by a GSDMD-dependent pathway, confirming previous reports (Evavold et al., 2018; Heilig et al., 2018). Some low-MW proteins, however, are retained in the cell due to osmoprotection. This may be explained by their physiological assembly into higher order structures or large protein complexes.

We show that lysosomal cargo and some mitochondrial proteins are released independently of cell lysis. The osmoprotection-independent extracellular presence of lysosomal lumen proteins with diverse MWs suggests an involvement of a vesicular release route. In contrast, the osmoprotection-sensitive release of both mitochondrial matrix and membrane proteins suggests that mitochondrial proteins enter the cytosol due to organellar damage upon inflammasome activation, followed by their exit along with cytosolic proteins by gasdermin pores. It will be interesting to elucidate the role of vesicular protein release from different cellular compartments during later stages of cell lysis, after pore formation.

PM repair mechanisms activated by membrane damage may further fine-tune paracrine programs by favoring the release of lysosomal cargo and small-MW proteins during sub-lytic inflammasome activation (Rühl et al., 2018).

Different forms of cell death use distinct mechanisms to control their paracrine programs. Pyroptosis is unique in its fast release of cDAMPs and slow release of pro-inflammatory cytokines IL-1β and IL-18. The execution of necroptosis, in contrast, is slower and accompanied by increased receptor shedding, which is not detected in pyroptosis, and decreased cytokine production. Whether distinct sets of proteins exit cells through GSDMD versus the necroptotic terminal effector-mixed lineage kinase domain-like (MLKL)-mediated PM perturbation remains to be determined (Petrie et al., 2017; Tanzer et al., 2020). Furthermore, the cell type specificity of protein exit mechanisms and accompanying paracrine programs are exciting topics for future investigations.

In conclusion, we have devised an MS-based experimental strategy to define the exit routes for each cellular protein. We demonstrated the utility of our approach by identifying multiple alarmins with known extracellular signaling capabilities to be released via cell-lysis-dependent and -independent pathways of pyroptosis. Our work serves as a valuable resource for the identification of proteins with as yet undescribed extracellular functions. Future studies should reveal how the differentially regulated sets of proteins direct paracrine immune responses under inflammatory conditions involving inflammasomes.

Figure 7. Dissection of constitutively expressed versus TLR-activation-induced cytokines and DAMPs

(A–C) Release of TNF-α (A) and IL-1β (B) as measured by ELISA or LDH (C) from supernatants of Caspase 1/11 DKO immortalized murine macrophages expressing an engineered caspase-1 system (Casp1ΔCard-FKBP), allowing its controlled dimerization, activation, and pyroptosis by AP20187 (AP) in the presence or absence of TLR4 and AP20187 activation. Data are represented as mean ± SD of three biological replicates.

(D and E) Volcano plots showing secreted proteins from differentially activated engineered Casp1ΔCard-FKBP-expressing cells. Pairwise secretome comparisons are shown between untreated and AP20187-activated cells to define constitutively released DAMPs and cytokines (D) TLR4 or TLR4 and AP20187-activated cells (E) to define differentially released cytokines and DAMPs that require induction by TLR4 signaling.

(F) Scatterplot of fold changes of released proteins between untreated and AP20187-activated cells versus TLR4 or TLR4 and AP20187-activated cells. Conventionally and unconventionally released cytokines are indicated by red and blue circles, respectively.

(G and H) Quantification of pyroptotic release of MIF (G) and Aimp1 (H) by ELISA and western blot, respectively.

(I) Heatmap of indicated conventionally secreted cytokines and pyroptotically released cDAMPs and iDAMPs or cytokines with mode of release as soluble or vesicle associated; osmoprotection or BFA dependency are indicated with the respective color coding.

See also Figures S1, S4, and S7 and Table S1.

STAR★METHODS

Detailed methods are provided in the online version of this paper and include the following:

- KEY RESOURCES TABLE
- RESOURCE AVAILABILITY
  - Lead contact
  - Materials availability
  - Data and code availability
- EXPERIMENTAL MODEL AND SUBJECT DETAILS
- METHOD DETAILS
  - Isolation and culture of murine bone marrow-derived macrophages
  - Generation of human monocyte-derived macrophages
  - Activation of BMDMs and human macrophages
  - Generation of cell lysates
  - Caspase 1 activity and cytotoxicity (LDH) assays
  - Enzyme-linked immunosorbent assay (ELISA)
  - Western blot
  - Immunostaining and fluorescent microscopy
  - P100 fraction/Extracellular vesicle isolation
  - Sample preparation for mass spectrometry
  - LC-MS/MS
- QUANTIFICATION AND STATISTICAL ANALYSIS
  - LC-MS/MS data analysis
  - Data preparation, quality control, and copy number estimation
  - Bioinformatics analysis of protein secretion signatures and receptor shedding

SUPPLEMENTAL INFORMATION

Supplemental information can be found online at https://doi.org/10.1016/j.celrep.2021.108826.

ACKNOWLEDGMENTS

We thank Matthias Mann for providing LC-MS/MS infrastructure and support. We thank Steven Dewitz, Korbinian Mayr, Mario Oroshi, Igor Paron, Christian Deiml, Bianca Splettstoesser, and Gaby Sowa for excellent technical assistance. Light microscopy was performed in the MPIB Imaging Facility. We thank Petr Broz for the GSDMD KO and Casp1/11 DKO Casp1ΔCard-FKBP iBMDMs. We thank all members of the Meissner, Zychlinsky, and Mann groups for helpful discussions. This work was funded by the Max Planck Society for the Advancement of Science and the Deutsche Forschungsgemeinschaft (DFG, German Research Foundation) project-IDs 165054336 (SFB 914), 360372040 (SFB 1335), and 408885537 (TRR 274). One or more of the authors of this paper self-identifies as a member of the LGBTQ+ community. The author list of this paper includes contributors from the location where the research was conducted who participated in the data collection, design, analysis, and/or interpretation of the work.

AUTHOR CONTRIBUTIONS

F.M. conceived the study. K.P. and F.M. designed experiments. K.P. performed experiments with help from S.E. and J.J.S. L.I.K. contributed experiments and analyses to Figures 1, 3, and S1–S4. K.P. analyzed data with suggestions from F.M. A.F. performed the receptor shedding analysis. K.P. and F.M. interpreted the data and wrote the manuscript.

DECLARATION OF INTERESTS

The authors declare no competing interests.

Received: July 24, 2020
Revised: November 25, 2020
Accepted: February 16, 2021
Published: March 9, 2021

REFERENCES

Aebersold, R., and Mann, M. (2016). Mass-spectrometric exploration of proteome structure and function. Nature *537*, 347–355.

Andrei, C., Dazzi, C., Lotti, L., Torrisi, M.R., Chimini, G., and Rubartelli, A. (1999). The secretory route of the leaderless protein interleukin 1beta involves exocytosis of endolysosome-related vesicles. Mol. Biol. Cell *10*, 1463–1475.

Arango Duque, G., and Descoteaux, A. (2014). Macrophage cytokines: involvement in immunity and infectious diseases. Front. Immunol. *5*, 491.

Baroja-Mazo, A., Compan, V., Martín-Sánchez, F., Tapia-Abellán, A., Couillin, I., and Pelegrín, P. (2019). Early endosome autoantigen 1 regulates IL-1β release upon caspase-1 activation independently of gasdermin D membrane permeabilization. Sci. Rep. *9*, 5788.

Bergsbaken, T., Fink, S.L., and Cookson, B.T. (2009). Pyroptosis: host cell death and inflammation. Nat. Rev. Microbiol. *7*, 99–109.

Bergsbaken, T., Fink, S.L., den Hartigh, A.B., Loomis, W.P., and Cookson, B.T. (2011). Coordinated host responses during pyroptosis: caspase-1-dependent lysosome exocytosis and inflammatory cytokine maturation. J. Immunol. *187*, 2748–2754.

Boucher, D., Monteleone, M., Coll, R.C., Chen, K.W., Ross, C.M., Teo, J.L., Gomez, G.A., Holley, C.L., Bierschenk, D., Stacey, K.J., et al. (2018). Caspase-1 self-cleavage is an intrinsic mechanism to terminate inflammasome activity. J. Exp. Med. *215*, 827–840.

Bronner, D.N., Abuaita, B.H., Chen, X., Fitzgerald, K.A., Nuñez, G., He, Y., Yin, X.M., and O'Riordan, M.X. (2015). Endoplasmic Reticulum Stress Activates the Inflammasome via NLRP3- and Caspase-2-Driven Mitochondrial Damage. Immunity *43*, 451–462.

Brough, D., Pelegrin, P., and Nickel, W. (2017). An emerging case for membrane pore formation as a common mechanism for the unconventional secretion of FGF2 and IL-1β. J. Cell Sci. *130*, 3197–3202.

Broz, P., and Dixit, V.M. (2016). Inflammasomes: mechanism of assembly, regulation and signalling. Nat. Rev. Immunol. *16*, 407–420.

Cai, Z., Zhang, A., Choksi, S., Li, W., Li, T., Zhang, X.M., and Liu, Z.G. (2016). Activation of cell-surface proteases promotes necroptosis, inflammation and cell migration. Cell Res. *26*, 886–900.

Chardin, P., and McCormick, F. (1999). Brefeldin A: the advantage of being uncompetitive. Cell *97*, 153–155.

Cox, J., and Mann, M. (2008). MaxQuant enables high peptide identification rates, individualized p.p.b.-range mass accuracies and proteome-wide protein quantification. Nat. Biotechnol. *26*, 1367–1372.

Cox, J., Neuhauser, N., Michalski, A., Scheltema, R.A., Olsen, J.V., and Mann, M. (2011). Andromeda: a peptide search engine integrated into the MaxQuant environment. J. Proteome Res. *10*, 1794–1805.

Cox, J., Hein, M.Y., Luber, C.A., Paron, I., Nagaraj, N., and Mann, M. (2014). Accurate proteome-wide label-free quantification by delayed normalization and maximal peptide ratio extraction, termed MaxLFQ. Mol. Cell. Proteomics *13*, 2513–2526.

Cypryk, W., Nyman, T.A., and Matikainen, S. (2018). From Inflammasome to Exosome-Does Extracellular Vesicle Secretion Constitute an Inflammasome-Dependent Immune Response? Front. Immunol. *9*, 2188.

Ding, J., Wang, K., Liu, W., She, Y., Sun, Q., Shi, J., Sun, H., Wang, D.C., and Shao, F. (2016). Pore-forming activity and structural autoinhibition of the gasdermin family. Nature *535*, 111–116.

DiPeso, L., Ji, D.X., Vance, R.E., and Price, J.V. (2017). Cell death and cell lysis are separable events during pyroptosis. Cell Death Discov. *3*, 17070.

Dupont, N., Jiang, S., Pilli, M., Ornatowski, W., Bhattacharya, D., and Deretic, V. (2011). Autophagy-based unconventional secretory pathway for extracellular delivery of IL-1β. EMBO J. *30*, 4701–4711.

Evavold, C.L., Ruan, J., Tan, Y., Xia, S., Wu, H., and Kagan, J.C. (2018). The Pore-Forming Protein Gasdermin D Regulates Interleukin-1 Secretion from Living Macrophages. Immunity *48*, 35–44.e6.

Fink, S.L., and Cookson, B.T. (2006). Caspase-1-dependent pore formation during pyroptosis leads to osmotic lysis of infected host macrophages. Cell. Microbiol. *8*, 1812–1825.

Finn, R.D., Coggill, P., Eberhardt, R.Y., Eddy, S.R., Mistry, J., Mitchell, A.L., Potter, S.C., Punta, M., Qureshi, M., Sangrador-Vegas, A., et al. (2016). The Pfam protein families database: towards a more sustainable future. Nucleic Acids Res. *44*, D279–D285.

Gong, T., Liu, L., Jiang, W., and Zhou, R. (2020). DAMP-sensing receptors in sterile inflammation and inflammatory diseases. Nat. Rev. Immunol. *20*, 95–112.

Heilig, R., Dick, M.S., Sborgi, L., Meunier, E., Hiller, S., and Broz, P. (2018). The Gasdermin-D pore acts as a conduit for IL-1β secretion in mice. Eur. J. Immunol. *48*, 584–592.

Hernández, S., Ferragut, G., Amela, I., Perez-Pons, J., Piñol, J., Mozo-Villarias, A., Cedano, J., and Querol, E. (2014). MultitaskProtDB: a database of multitasking proteins. Nucleic Acids Res. *42*, D517–D520.

Jeffery, C.J. (1999). Moonlighting proteins. Trends Biochem. Sci. *24*, 8–11.

Kaisho, T., and Akira, S. (2000). Critical roles of Toll-like receptors in host defense. Crit. Rev. Immunol. *20*, 393–405.

Kayagaki, N., Stowe, I.B., Lee, B.L., O'Rourke, K., Anderson, K., Warming, S., Cuellar, T., Haley, B., Roose-Girma, M., Phung, Q.T., et al. (2015). Caspase-11 cleaves gasdermin D for non-canonical inflammasome signalling. Nature *526*, 666–671.

Kayagaki, N., Warming, S., Lamkanfi, M., Walle, L.V., Louie, S., Dong, J., Newton, K., Qu, Y., Liu, J., Heldens, S., et al. (2011). Non-canonical inflammasome activation targets caspase-11. Nature *479*, 117–121.

Kelstrup, C.D., Bekker-Jensen, D.B., Arrey, T.N., Hogrebe, A., Harder, A., and Olsen, J.V. (2018). Performance Evaluation of the Q Exactive HF-X for Shotgun Proteomics. J. Proteome Res. *17*, 727–738.

Lamkanfi, M., Sarkar, A., Vande Walle, L., Vitari, A.C., Amer, A.O., Wewers, M.D., Tracey, K.J., Kanneganti, T.-D., and Dixit, V.M. (2010). Inflammasome-dependent release of the alarmin HMGB1 in endotoxemia. J. Immunol. *185*, 4385–4392.

Lammert, C.R., Frost, E.L., Bellinger, C.E., Bolte, A.C., McKee, C.A., Hurt, M.E., Paysour, M.J., Ennerfelt, H.E., and Lukens, J.R. (2020). AIM2 inflammasome surveillance of DNA damage shapes neurodevelopment. Nature *580*, 647–652.

Larance, M., and Lamond, A.I. (2015). Multidimensional proteomics for cell biology. Nat. Rev. Mol. Cell Biol. *16*, 269–280.

Liu, X., Zhang, Z., Ruan, J., Pan, Y., Magupalli, V.G., Wu, H., and Lieberman, J. (2016). Inflammasome-activated gasdermin D causes pyroptosis by forming membrane pores. Nature *535*, 153–158.

Lobb, R.J., Becker, M., Wen, S.W., Wong, C.S., Wiegmans, A.P., Leimgruber, A., and Möller, A. (2015). Optimized exosome isolation protocol for cell culture supernatant and human plasma. J. Extracell. Vesicles *4*, 27031.

Loomis, W.P., den Hartigh, A.B., Cookson, B.T., and Fink, S.L. (2019). Diverse small molecules prevent macrophage lysis during pyroptosis. Cell Death Dis. *10*, 326.

Lopez-Castejon, G., and Brough, D. (2011). Understanding the mechanism of IL-1β secretion. Cytokine Growth Factor Rev. *22*, 189–195.

MacCorkle, R.A., Freeman, K.W., and Spencer, D.M. (1998). Synthetic activation of caspases: artificial death switches. Proc. Natl. Acad. Sci. USA *95*, 3655–3660.

Marshall, J.D., Aste-Amézaga, M., Chehimi, S.S., Murphy, M., Olsen, H., and Trinchieri, G. (1999). Regulation of human IL-18 mRNA expression. Clin. Immunol. *90*, 15–21.

Martín-Sánchez, F., Diamond, C., Zeitler, M., Gomez, A.I., Baroja-Mazo, A., Bagnall, J., Spiller, D., White, M., Daniels, M.J.D., Mortellaro, A., et al. (2016). Inflammasome-dependent IL-1β release depends upon membrane permeabilisation. Cell Death Differ. *23*, 1219–1231.

Meissner, F., Scheltema, R.A., Mollenkopf, H.J., and Mann, M. (2013). Direct proteomic quantification of the secretome of activated immune cells. Science *340*, 475–478.

Menu, P., Mayor, A., Zhou, R., Tardivel, A., Ichijo, H., Mori, K., and Tschopp, J. (2012). ER stress activates the NLRP3 inflammasome via an UPR-independent pathway. Cell Death Dis. *3*, e261.

Mitchell, P.S., Sandstrom, A., and Vance, R.E. (2019). The NLRP1 inflammasome: new mechanistic insights and unresolved mysteries. Curr. Opin. Immunol. *60*, 37–45.

Mohamed, M.M., and Sloane, B.F. (2006). Cysteine cathepsins: multifunctional enzymes in cancer. Nat. Rev. Cancer *6*, 764–775.

Monteleone, M., Stow, J.L., and Schroder, K. (2015). Mechanisms of unconventional secretion of IL-1 family cytokines. Cytokine *74*, 213–218.

Nagaraj, N., Kulak, N.A., Cox, J., Neuhauser, N., Mayr, K., Hoerning, O., Vorm, O., and Mann, M. (2012). System-wide perturbation analysis with nearly complete coverage of the yeast proteome by single-shot ultra HPLC runs on a bench top Orbitrap. Mol. Cell Proteomics *11*, M111.013722.

Ng, F., and Tang, B.L. (2016). Unconventional Protein Secretion in Animal Cells. Unconventional Protein Secretion (Springer New York), pp. 31–46.

Nickel, W., and Rabouille, C. (2009). Mechanisms of regulated unconventional protein secretion. Nat. Rev. Mol. Cell Biol. *10*, 148–155.

Olson, O.C., and Joyce, J.A. (2015). Cysteine cathepsin proteases: regulators of cancer progression and therapeutic response. Nat. Rev. Cancer *15*, 712–729.

Petrie, E.J., Hildebrand, J.M., and Murphy, J.M. (2017). Insane in the membrane: a structural perspective of MLKL function in necroptosis. Immunol. Cell Biol. *95*, 152–159.

Rathkey, J.K., Zhao, J., Liu, Z., Chen, Y., Yang, J., Kondolf, H.C., Benson, B.L., Chirieleison, S.M., Huang, A.Y., Dubyak, G.R., et al. (2018). Chemical disruption of the pyroptotic pore-forming protein gasdermin D inhibits inflammatory cell death and sepsis. Sci. Immunol. *3*, eaat2738.

Rieckmann, J.C., Geiger, R., Hornburg, D., Wolf, T., Kveler, K., Jarrossay, D., Sallusto, F., Shen-Orr, S.S., Lanzavecchia, A., Mann, M., and Meissner, F. (2017). Social network architecture of human immune cells unveiled by quantitative proteomics. Nat. Immunol. *18*, 583–593.

Rubartelli, A., Cozzolino, F., Talio, M., and Sitia, R. (1990). A novel secretory pathway for interleukin-1 beta, a protein lacking a signal sequence. EMBO J. *9*, 1503–1510.

Rühl, S., Shkarina, K., Demarco, B., Heilig, R., Santos, J.C., and Broz, P. (2018). ESCRT-dependent membrane repair negatively regulates pyroptosis downstream of GSDMD activation. Science *362*, 956–960.

Sáenz, J.B., Sun, W.J., Chang, J.W., Li, J., Bursulaya, B., Gray, N.S., and Haslam, D.B. (2009). Golgicide A reveals essential roles for GBF1 in Golgi assembly and function. Nat. Chem. Biol. *5*, 157–165.

Scheltema, R.A., and Mann, M. (2012). SprayQc: a real-time LC-MS/MS quality monitoring system to maximize uptime using off the shelf components. J. Proteome Res. *11*, 3458–3466.

Scheltema, R.A., Hauschild, J.-P., Lange, O., Hornburg, D., Denisov, E., Damoc, E., Kuehn, A., Makarov, A., and Mann, M. (2014). The Q Exactive HF, a Benchtop mass spectrometer with a pre-filter, high-performance quadrupole and an ultra-high-field Orbitrap analyzer. Mol. Cell. Proteomics *13*, 3698–3708.

Stow, J.L., Low, P.C., Offenhäuser, C., and Sangermani, D. (2009). Cytokine secretion in macrophages and other cells: pathways and mediators. Immunobiology *214*, 601–612.

Stutz, A., Horvath, G.L., Monks, B.G., and Latz, E. (2013). ASC speck formation as a readout for inflammasome activation. Methods Mol. Biol. *1040*, 91–101.

Swanson, K.V., Deng, M., and Ting, J.P.Y. (2019). The NLRP3 inflammasome: molecular activation and regulation to therapeutics. Nat. Rev. Immunol. *19*, 477–489.

Tanzer, M.C., Frauenstein, A., Stafford, C.A., Phulphagar, K., Mann, M., and Meissner, F. (2020). Quantitative and Dynamic Catalogs of Proteins Released during Apoptotic and Necroptotic Cell Death. Cell Rep. *30*, 1260–1270.e5.

Tapia, V.S., Daniels, M.J.D., Palazón-Riquelme, P., Dewhurst, M., Luheshi, N.M., Rivers-Auty, J., Green, J., Redondo-Castro, E., Kaldis, P., Lopez-Castejon, G., and Brough, D. (2019). The three cytokines IL-1β, IL-18, and IL-1α share related but distinct secretory routes. J. Biol. Chem. *294*, 8325–8335.

Tusher, V.G., Tibshirani, R., and Chu, G. (2001). Significance analysis of microarrays applied to the ionizing radiation response. Proc. Natl. Acad. Sci. USA *98*, 5116–5121.

Tyanova, S., Temu, T., Sinitcyn, P., Carlson, A., Hein, M.Y., Geiger, T., Mann, M., and Cox, J. (2016). The Perseus computational platform for comprehensive analysis of (prote)omics data. Nat. Methods *13*, 731–740.

Weischenfeldt, J., and Porse, B. (2008). Bone Marrow-Derived Macrophages (BMM): Isolation and Applications. CSH Protoc. *2008*, pdb.prot5080-pdb.prot5080.

Yatim, N., Cullen, S., and Albert, M.L. (2017). Dying cells actively regulate adaptive immune responses. Nat. Rev. Immunol. *17*, 262–275.

Zhang, M., Kenny, S.J., Ge, L., Xu, K., and Schekman, R. (2015). Translocation of interleukin-1β into a vesicle intermediate in autophagy-mediated secretion. eLife *4*, e11205.

Zhang, Z., Meszaros, G., He, W.T., Xu, Y., de Fatima Magliarelli, H., Mailly, L., Mihlan, M., Liu, Y., Puig Gámez, M., Goginashvili, A., et al. (2017). Protein kinase D at the Golgi controls NLRP3 inflammasome activation. J. Exp. Med. *214*, 2671–2693.

STAR★METHODS

KEY RESOURCES TABLE

REAGENT or RESOURCE	SOURCE	IDENTIFIER
Antibodies		
Anti-mouse Aimp1	Novus Biologicals	Cat#NBP2-27206SS
Anti-GAPDH	Cell Signaling Technology	Cat#8884s; RRID: AB_11129865
Anti-PDI	Cell Signaling Technology	Cat#3501; RRID: AB_2156433
Anti-Rcas1	Cell Signaling Technology	Cat#12290; RRID: AB_2736985
Anti-Ctsb	Cell Signaling Technology	Cat#31718; RRID: AB_2687580
Anti-β-Actin	Cell Signaling Technology	Cat#8457; RRID: AB_10950489
Anti-Vamp8	Cell Signaling Technology	Cat#13060; RRID: AB_2798103
Anti-Lamp1	Cell Signaling Technology	Cat#3243; RRID: AB_2134478
Anti-Asc	Sigma-Aldrich	04-147; RRID: AB_1977033
F(ab')2-AF647	Thermo Fisher Scientific	A21237; AB_1500743
HRP-linked anti mouse IgG	Cyvita	Cat#NXA931; RRID: AB_772209
HRP-linked anti rabbit IgG	Cyvita	Cat#NA934; RRID: AB_772206
Biological samples		
Buffy Coats	Blood donations to the red cross	"Blutspendedienst des Bayerischen Roten Kreuzes gemeinnützige GmbH"
Chemicals, peptides, and recombinant proteins		
Lipopolysaccharide (LPS) from Salmonella typhimurium S-form	Enzo Life Sciences	ALX-581-013-L002
Nigericin sodium salt from Streptomyces hygroscopicus	Thermo Fisher Scientific	N1495
Adenosine 5′-triphosphate disodium salt hydrate (ATP)	Sigma	Cat#7699
Lethal factor	List Biologicals	Cat#172B
Protective antigen	List Biologicals	Cat#171E
AP20187/B/B homodimerizor	Takara Biotech	Cat#635058
Brefeldin A	Cell Signaling Technology	Cat#9972
Golgicide A	Sigma-Aldrich	G0923
Glybenclamide/Glyburide	Novus Biologicals	Cat#NBP2-30141
Draq5	Thermo Fisher Scientific	Cat#62252
L-Alanine	Sigma-Aldrich	A7469
Glycine	Sigma-Aldrich	G7126
hM-CSF	Cell Signaling Technology	Cat#8929LC
Red blood cell lysis buffer	Sigma-Aldrich	R7757
Histopaque-1077	Sigma-Aldrich	10771
Heat inactivated Fetal Bovine Serum	Invitrogen	10270106
Penicillin/Streptomycin	Invitrogen	15140122
RPMI medium	Invitrogen	61870044
DME medium	Invitrogen	31966047
Phenol red free DMEM	Thermo Fisher Scientific	31053044
Urea	Sigma	45128-500 g
Thiourea	Sigma	T8656-500 g
Trizma	Sigma	T1503-1kg
Dithiothreitol (DTT)	Sigma	D0632-100 g

(*Continued on next page*)

Continued

REAGENT or RESOURCE	SOURCE	IDENTIFIER
Chloroacetamide (CAA)	Sigma	C0267-100 g
Iodoacetamide (IAA)	Sigma	I6125-100 g
Ammonium bicarbonate	Sigma	A6141
Trypsin	Sigma	T6567-1mg
Lys-C	Wako Chemicals	Cat#129-02541
DMSO	Sigma	D2650-100ml
Acetone	Fisher Chemical	Cat#67-64-1
Acetonitrile	VWR	Cat#20048320
Trifluoroacetic acid	Merck	Cat#8082600100
Formic acid	Merck	Cat#1002641000
PBS	GIBCO	Cat#14190-094
Tween	Acros	Cat#233360010
EDTA	Sigma	03677-500 g
BSA	Serva	Cat#11930.03
Glycerol	Sigma	G5516-1L
Sodium dodecyl sulfate (SDS)	Roth	Cat#CN30.3
Sodium deoxycholate (SDC)	Sigma	30970-100 g
Sodium chloride (NaCl)	VWR	Cat#27810.295
NuPAGE LDS Sample Buffer (4x)	Invitrogen	NP0007
Puromycin	Invivogen	Ant-pr-5
Critical commercial assays		
CytoTox 96 Non-Radioactive Cytotoxicity Assay	Promega	G1780
Human Tnf ELISA kit	R&D Systems	Cat#DY210
Human IL1b ELISA kit	R&D Systems	Cat#DY201
Mouse Tnf ELISA kit	R&D Systems	Cat#DY410
Mouse IL1b ELISA kit	R&D Systems	Cat#DY401
Mouse Mif ELISA kit	R&D Systems	Cat#DY1978
Caspase-Glo® 1 Inflammasome Assay	Promega	G9951
Human Monocyte Isolation Kit II	Miltenyi Biotec	Cat#130-091-153
Deposited data		
Raw Mass Spectrometry Data Files	This paper	ProteomeXchange Consortium via the PRIDE partner repository, with the dataset identifier PXD018659
Experimental models: organisms/strains		
C57BL/6J wild type mice (WT)	The Jackson Laboratory	Cat#000664
Casp1/11 DKO, strain B6.129S2-Casp1tm1SeshCasp11del/J	BASF	N/A
129S4/SvJae	The Jackson Laboratory	Cat#009104
Experimental models: cell lines		
GSDMD −/− iBMDMs	Dr. Petr Broz	Heilig et al., 2018
Casp1/11 DKO iBMDMs reconstituted with Casp1ΔCard-FKBP	Dr. Petr Broz	Boucher et al., 2018
L929 cells	ATCC	ATCC CCL-1
Software and algorithms		
MaxQuant	Cox and Mann, 2008; Version 1.5.0.38	https://www.biochem.mpg.de/5111795/maxquant
Perseus	Tyanova et al., 2016; Version 1.5.3.0	https://www.biochem.mpg.de/5111810/perseus

(*Continued on next page*)

Continued

REAGENT or RESOURCE	SOURCE	IDENTIFIER
XCalibur	Thermo Scientific	https://www.thermofisher.com/order/catalog/product/OPTON-30487
R	N/A	https://www.r-project.org/
ImageJ	N/A	https://imagej.nih.gov/ij/
Adobe Illustrator	N/A	https://www.adobe.com/de/products/illustrator.html
PRIDE	N/A	https://www.ebi.ac.uk/pride/archive/

RESOURCE AVAILABILITY

Lead contact

Further information and requests for resources should be directed to and will be fulfilled by the Lead Contact, Felix Meissner (meissner@biochem.mpg.de).

Materials availability

This study did not generate new unique materials and reagents.

Data and code availability

The datasets generated in this study are available via ProteomeXchange with identifier PXD018659.

EXPERIMENTAL MODEL AND SUBJECT DETAILS

Experiments described in this study are performed with the mouse and human primary macrophages or immortalized mouse macrophages.

C57BL/6J wild-type mice (WT) and 129S4/SvJae mice (WT) were obtained from The Jackson Laboratory. Caspase-1/11 double knockout mice (Casp1/11 DKO, strain B6.129S2-Casp1^{tm1Sesh}Casp11^{del}/J) were kindly provided by BASF. This strain was originally generated as Casp1 deficient mice but is effectively Casp1/11 double deficient due to an additional mutation in the Casp11 gene locus in the 129S2 background used for ES cell generation (Kayagaki et al., 2011). Both mouse strains were housed under specific-pathogen-free (SPF) conditions on a 12-hour light/dark cycle in the animal facility of the Max Planck Institute for Infection Biology OR Biochemistry. 10-12 week old male mice were sacrificed by cervical dislocation and directly used for bone marrow-derived macrophage preparation. Animal experiments were performed according to the German Animal Protection Law.

Human primary macrophages were generated by isolating PBMCs from buffy coats (generated from blood donations to the Red Cross or Blutspendedienst des Bayerischen Roten Kreuzes gemeinnützige GmbH) using Histopaque-1077 (Sigma-Aldrich, 10771). Gender or age of donors is not disclosed by the Red Cross. Monocytes were isolated using a monocyte isolation kit (Miltenyi Biotec, 130-091-153). Immortalized GSDMD KO and Casp1/11 DKO iBMDMs reconstituted with Casp1ΔCard-FKBP were a kind gift from Petr Broz (Boucher et al., 2018; Heilig et al., 2018).

METHOD DETAILS

Isolation and culture of murine bone marrow-derived macrophages

Bone marrow-derived macrophages (BMDMs) were prepared as described elsewhere (Weischenfeldt and Porse, 2008). In brief, bone marrow was collected from the femurs and tibiae of 8-12 weeks old male mice and filtered through a 70 μm nylon mesh filter. 5×10^6 to 1×10^7 bone marrow cells were plated on sterile, non-tissue culture treated Petri plates for a period of 7 days in macrophage differentiation medium DMEM supplemented with 10% (v/v) FCS and 20% (v/v) M-CSF-containing medium. Medium was replenished on day 3 of culture. M-CSF-conditioned medium was collected from L-929 cells. Cells were lifted from plates by incubating in cold PBS and re-plated for experiments.

Immortalized Casp1/11 DKO BMDMs reconstituted with Casp1ΔCard-FKBP were cultured in macrophage differentiation medium supplemented with 10ug/ml Puromycin.

Generation of human monocyte-derived macrophages

Blood was drawn with S-Monovette 9ml K2E-Gel (#02.1333.001, Sarstedt) from healthy volunteers according to the WMA Declaration of Helsinki and the Department of Health and Human Services Belmont Report. Donors provided informed consent and all samples were collected with approval from the ethics committee. Blood was diluted 1:1 with PBS and centrifuged over Histopaque-1077 (#10771, Sigma) at 400 g for 40 min. After centrifugation, the peripheral blood mononuclear cell (PBMC) fraction was

collected and washed three times with PBS followed by centrifugation at 200 g for 15 min to remove platelets. Red blood cells were lysed with RBC lysis buffer (Sigma) for 3 min. PBMCs were washed again with PBS supplemented with 0.5% (w/v) bovine serum albumin (BSA) and 2 mM EDTA. Monocytes were isolated by negative selection using the human Monocyte Isolation Kit II (#130-091-153, Miltenyi Biotec) according to the manufacturer's instructions. For the generation of macrophages, 2×10^7 isolated monocytes were plated on sterile, non-tissue culture treated Petri plates for a period of 7 days in RPMI 1640 supplemented with 10% (v/v) FCS, and 50 ng/mL human M-CSF (#8929LC, Cell Signaling). Medium was refreshed on day 3 of culture. On day 7, cells were lifted from plates by incubating in cold PBS and re-plated for experiments.

Activation of BMDMs and human macrophages

All cells were grown, maintained and activated at 37°C and 5% CO_2 in a water-jacketed incubator. 1×10^6 WT or *Casp1/11* DKO murine macrophages were plated per 12-well in DMEM, 10% (v/v) FCS (DMEM complete medium) one day prior to stimulation. All BMDMs were primed with 200 ng/mL LPS from *Salmonella* Typhimurium for 2 h or left untreated and subsequently washed three times with serum- and phenol red-free DMEM supplemented with 2 mM L-glutamine (DMEM minimal medium). For the time course experiment (Dataset 1), cells were preincubated with 0 or 100 μM glyburide (#NBP2-30141, Novus Biologicals) for 15-30min before 2 mM ATP (#7699, Sigma) or 10 μM nigericin (N1495, Invitrogen) were added for 15, 30, 45, and 60 min. Lethal factor and protective antigen were added at 1ug/ml. To inhibit conventional protein secretion (Dataset 3), 0-2 μg/mL brefeldin A were added for the last 15-30 min of priming. After washing 0-2ug/ml BFA along with 5 mM ATP or 15 μM nigericin were added for 30-45 min. For osmoprotection experiments (Dataset 2), cells were incubated with 20-30mM L-alanine or Glycine in DMEM minimal medium for 1 h after priming and washing, before 5 mM ATP or 15 μM nigericin were added for 30-45 min. AP20187 was added at 100nM for 160min.

Human macrophages (Datasets 5 and 6) were seeded at a density of 1×10^6 cells per 12-well in RPMI 1640 containing 10% (v/v) FCS, 2 mM L-glutamine, MEM NEAA, 100 U/mL penicillin, 100 μg/mL streptomycin (RPMI complete medium) one day before activation. Cells were primed with 200 ng/mL LPS for 2 h in complete medium. 1 μg/mL Brefeldin A was added for the last 30 min of priming before cells were washed three times with serum- and phenol red-free RPMI 1640 supplemented with 2 mM HEPES and 2 mM L-glutamine (RPMI minimal medium). After washing, cells were incubated with 1 μg/mL brefeldin A and 2 mM ATP or 10 μM nigericin for 30-45 min.

All activation experiments were performed in three technical replicates. Cell supernatants were centrifuged at 400 g for 5 min or sterile filtered to remove cell debris and directly used for LDH assay or stored at −80°C until ELISA and sample preparation. After removal of supernatants, untreated and LPS treated samples were used for the generation of total cell lysates (Datasets 4 and 6).

Generation of cell lysates

To generate total lysates for mass spectrometry, cells were washed with PBS and resuspended in 8 M urea in 40 mM HEPES pH 8 and frozen at −80°C until sample preparation.

Caspase 1 activity and cytotoxicity (LDH) assays

Caspase 1 activity was measured using the Caspase-Glo® 1 Inflammasome Assay as per the manufacturer's instructions. Cell death was measured by means of lactate dehydrogenase (LDH) release into the cell supernatant using the CytoTox 96 Non-Radioactive Cytotoxicity Assay (#G1780, Promega). In brief, 50 μL cell supernatant were incubated with 50 μL LDH substrate and incubated in the dark at 37°C for 15 to 30 min. The enzymatic reaction was stopped by adding 50 μL stop solution. Whole cell lysates generated from unstimulated cells incubated with medium supplemented with 1.2% (v/v) Triton X-100 for 30 min served as a reference for maximal cell death. Cell death was calculated as follows: (LDH release/LDH whole cell lysate) × 100.

Enzyme-linked immunosorbent assay (ELISA)

Human and mouse IL-1β, TNF-α and MIF in cell supernatants were measured with ELISA Kits purchased from R and D Systems (#DY201, #DY401, #DY210, #DY410, #DY1978) according to the manufacturer's instructions.

Western blot

Samples were prepared by lysing cells in lysis buffer (1% Triton X-100, 50mM Tris-Hcl pH 7.5, 150mM NaCl. Nuclei were removed by centrifugation (10 min, 1000 × g). Proteins from cell supernatants were precipitated with acetone (final concentration 80%) o/n at −20C. Protein pellets obtained after centrifugation at 3900 x g were solubilized in 2% SDS, 50mM Tris-HCl pH 7.5. Protein concentration was normalized after measurement with a bicinchoninic acid assay (BCA; Thermo Fisher Scientific). Samples were reduced and denatured by adding NuPAGE LDS Sample Buffer (4 ×) and NuPAGE Sample Reducing Agent (10 ×) (both from Thermo Fisher) and heating at 85 °C for 10 min. Proteins were separated by 4%–12% SDS-PAGE in precast gels (Novex; Invitrogen) with MOPS buffer (Novex; Invitrogen). Proteins were transferred onto Immobilon-FL PVDF membranes (Millipore) and nonspecific binding was blocked with 5% non-fat milk in Tris-buffered saline with 0.1% Tween-20 (TBST) for 1 h, followed by overnight incubation with specific primary antibodies in 5% BSA in TBST as per the manufacturer's instructions.

The following primary antibodies were used: PDI (1:1000, CST #3501), Rcas1 (1:1000, CST #12290), Ctsb (1:1000, CST #31718), β-Actin (1:1000, CST #8457), IL-1β (R and D systems, #DY401 ELISA detection antibody 1:50), Aimp1 (NBP2-27206SS), Gapdh (1:1000, CST #8884s), Vamp8 (1:100, CST #13060), Lamp1 (1:100, CST #3243). Membranes were washed 3X and incubated in

HRP linked anti-mouse (Cytiva #NXA931) or rabbit IgG antibodies (Cytiva #NA934) in 5% BSA in TBS-T for 1 h at room temperature (RT) followed by washing 3X in TBS-T

Immunostaining and fluorescent microscopy

BMDMs were fixed with 4% formaldehyde and stained for ASC (Milipore 2EI-7, Thermo Fisher F(ab')2-AF647) as per the manufacturer's instructions. Nuclei were counterstained using Draq5. Microscopy was performed in the MPIB imaging facility. Cells were imaged using a GE Deltavision Elite (Cytiva Life Sciences) epifluorescence microscope. Images were quantified as described previously using ImageJ (Stutz et al., 2013).

P100 fraction/Extracellular vesicle isolation

2e7 bone marrow macrophages were treated for three hours with LPS followed by 45min with Nigericin or ethanol a control. Supernatants were collected and spun for 5 minutes at 500 x g. followed by another spin 30 minutes at 10,000 x g. Supernatants were concentrated 5X using 30kD cellulose filters and the retentates were collected and spun for 60 minutes at 100,000 x g to obtain extracellular vesicle P100 fraction. The pellets were washed with ice cold PBS and again centrifuged for 60 minutes at 100,000 x g. The resulting pellet was lysed in 8 M Urea with 50 mM Tris (pH8), reduced with 10 mM DTT, alkylated with 40 mM CAA and digested for 2 hours with lysC (1 μg/sample) before 1:4 dilution with 50 mM ammonium bicarbonate and the addition of trypsin (1 μg/sample). Trypsin and lysC digestion occurred over night at RT and peptides were cleaned up by C18 stage tipping.

Sample preparation for mass spectrometry

Total lysates were diluted to a final urea concentration of 2 M and sonicated on ice for 15 min (level 5, Bioruptor, Diagenode). Cell supernatants (400 μL each) were denatured with 2 M urea in 10 mM HEPES pH 8. Proteins of both sample types were reduced with 10 mM dithiotreitol for 30 min at RT followed by alkylation with 55 mM iodoacetamide for 20 min at RT in the dark. Remaining iodoacetamide was quenched with 100 mM thiourea. Proteins were digested with 1 μg LysC (#129-02541, Wako Chemicals) at RT for 3 h and 1 μg trypsin (#T6567, Sigma) at RT overnight. Protein digestion was stopped with 0.6% (v/v) trifluoroacetic acid and 2% (v/v) acetonitrile before peptides were loaded onto reversed phase C18 StageTips (#2215, 3M™ Empore™, IVA Analysentechnik). Supernatants and 50 μg of total lysates were loaded onto the C18 StageTips. Peptides were desalted using 0.5% (v/v) acetic acid and subsequently eluted from the C18 StageTips with 50 μL 80% (v/v) acetonitrile in 0.5% (v/v) acetic acid. After concentrating and drying in a SpeedVac (Thermo Scientific), peptides were resuspended in 10 μL 2% (v/v) acetonitrile, 0.1% (v/v) trifluoroacetic acid in 0.5% (v/v) acetic acid and stored at −20°C until mass spectrometric analysis.

LC-MS/MS

Peptide mixtures were analyzed in a single-run liquid chromatography mass spectrometry (LC-MS/MS) format (Nagaraj et al., 2012). Each peptide mixture was loaded onto a C18-reversed phase column (20 cm long for supernatants and 50 cm long for total lysates, 75 μm inner diameter) and separated with a non-linear gradient of 2 - 60% buffer B (80% (v/v) acetonitrile in 0.1% (v/v) formic acid) at a flow rate of 250 nL/min over 107 min for supernatants and 180 min for total lysates using a nanoflow UHPLC instrument (Easy-nLC 1200, Thermo Scientific). Chromatography columns (#TSP075375, Composite Metal Service Ltd.) were packed at the MPI of Biochemistry with ReproSil-Pur 120 C18-AQ 1.9 μm resin (#r119.aq., Dr. Maisch GmbH) in methanol. Chromatography and column oven (Sonation GmbH) temperature were controlled and monitored in real-time with SprayQC (Scheltema and Mann, 2012). Column oven temeprature was set to 40°C for supernatants and 55°C for total lysates. Separated peptides were analyzed on a benchtop quadrupole-Orbitrap instrument (Q Exactive HF/HFx mass spectrometer, Thermo Scientific) with a nanoelectrospray ion source (Thermo Scientific), which was coupled on-line to the liquid chromatography instrument.

The mass spectrometer was operated in a data dependent mode with a survey scan range of 300-1650 m/z and a resolution of 60,000 at m/z 200. Up to the 10 most abundant precursor ions with charge states 2 to 5 were isolated for higher-energy collisional dissociation (HCD) with Thomson (Th) isolation windows of 1.4 m/z for secretomes and 1.8 m/z for total proteomes. Normalized collision energies (NCE) for HCD were 26 (proteomes) and 27 (secretomes), respectively. Fragmentation spectra were acquired with a resolution of 15,000 at m/z 200. Dynamic exclusion duration of sequenced peptides was set to 20 s (secretomes) or 30 s (proteomes) to reduce repeated peptide sequencing. Maximum ion injection times were 20 ms for the full MS scan and 80 ms (secretomes) or 55 ms (proteomes) for the MS/MS scan. Automatic gain control (AGC, ion target values) was set to 3e6 for the survey and 1e5 for the MS/MS scan. MS data were acquired as described previously using the Xcalibur software (Thermo Scientific) (Meissner et al., 2013).

QUANTIFICATION AND STATISTICAL ANALYSIS

LC-MS/MS data analysis

Protein identification and quantification from MS raw files was performed separately for the murine and human datasets using the computational proteomics platform MaxQuant (software version 1.5.5.2 or 1.6.2.1) (Cox and Mann, 2008). Murine and human MS/MS spectra were searched against the respective UniProt FASTA databases and a common contaminant database by the implemented Andromeda search engine (Cox et al., 2011). Secretomes and proteomes of all murine and all human datasets, respectively, were analyzed together. To avoid matching between different sample types, secretomes were set to fraction 1 and parameter

group 0 and total lysates to fraction 3 and parameter group 1. The used digestion mode was Trypsin/P with a minimum peptide length of 7 amino acids and a maximum of two missed cleavages. Cysteine carbamidomethylation was set as fixed and methionine oxidation and N-terminal acetylation as variable modifications. False discovery rates (FDR) were 1% at the peptide and protein level. Peptide identification was performed with an allowed initial precursor mass deviation up to 4.5 ppm and an allowed fragment mass deviation of 20 ppm. Protein identifications required one unique or razor peptide. For nonlinear retention time alignment of all samples, the "Match between runs" option of MaxQuant was used. The time windows for matching peptide identifications across different samples and to search for the best alignment function were set to 0.7 min and 20 min. For label-free quantification (LFQ) via MaxLFQ, a minimum ratio count of 1 was used and Fast LFQ enabled with a minimum of 3 and an average of 6 neighbors (Cox et al., 2014).

Data preparation, quality control, and copy number estimation

Data was analyzed with the Perseus computational platform (version 1.5.5.5) and the statistical software environment R and R Studio, respectively (Tyanova et al., 2016). The integrated graphics device or the package "ggplot2" in R Studio were used to visualize data. Proteins matching to the reversed or contaminants database as well as peptides only identified by side modification were excluded from the analysis. Data were additionally filtered to contain at least two valid values per protein identification in at least one group of replicates. The number of identified protein groups per condition and the Pearson correlation between technical replicates were determined and subsequently missing values were replaced. Missing values were imputed separately for secretomes and proteomes by a Gaussian distribution with a 30% width relative to the standard deviation of the measured values and a downshift of the mean by 1.8 standard deviations of the valid data. To assess the accuracy of the mass spectrometry approach, MS raw intensities and LFQ values were correlated (Pearson) to ELISA values for TNF-α and IL-1β using pairwise complete observations. By analogy, the Pearson correlation of LDH release and the summed MS raw or LFQ intensities of all proteins annotated as "cytoplasm," "cytoplasmic part," "intracellular," or "intracellular part" (cytosolic proteins) by the Gene Ontology (GO) term cellular component (GOCC) was calculated Of note, the label-free quantification technology MaxLFQ that in addition to peptide intensity information involves various normalization steps of the LC MS/MS runs to make protein amounts between different samples more comparable showed overall a much weaker correlation to the alternative (antibody and enzyme-based) quantification methods (Figures S2G–S2J). One reason being that the assumed requirements for MaxLFQ calculation, e.g., that protein compositions do not show major differences across different samples, are not fulfilled in our datasets. Hence, protein amounts were determined by label-free quantification using the summed raw intensities of the MS1 signal of each eluting peptide for all further analyses.

Bioinformatics analysis of protein secretion signatures and receptor shedding

To investigate differences in conventional and unconventional protein secretion from activated macrophages on a global scale we pairwise compared secretomes of differentially treated macrophages by calculating the ratios of individual protein abundances. A parametric two-tailed welch's t test with a permutation-based false discovery rate (FDR) of 5% and a S_0 parameter of 1 was employed to identify proteins that significantly differed in abundance (Tusher et al., 2001). Secretory signatures were functionally characterized by annotation enrichment analysis using annotations from the UniProt Keywords and Pfam protein domain databases (Finn et al., 2016). Enrichment factors were calculated with Fisher's exact test. All annotations with intersection sizes greater than 3 and p values less than 0.00025 were considered.

To analyze pyroptosis dependent receptor shedding, proteins were prefiltered by Uniprot Keywords 'Receptors' and their corresponding peptides were annotated "extracellular" and "intracellular" via Uniprot Keywords, respectively. Peptide intensities were logarithmized and normalized to LPS primed untreated conditions. A two-tailed t test was performed between extracellular and intracellular peptides of all receptors (Figure S6A) and selected receptors (Figures S6B and S6C) and significance was denoted by asterisks (*$p < 0.05$, **$p < 0.01$, ***$p < 0.001$, ****$p < 0.0001$).